



The Compact Muon Solenoid Experiment

CMS Note

Mailing address: CMS CERN, CH-1211 GENEVA 23, Switzerland



September 24, 2012

Searches for beyond-the-standard model physics in events with a Z boson, jets and missing transverse energy

D. Barge, C. Campagnari, D. Kovalskyi, V. Krutelyov

University of California, Santa Barbara, USA

W. Andrews, G. Cerati, D. Evans, F. Golf, I. MacNeill, S. Padhi, Y. Tu, F. Würthwein, A. Yagil, J. Yoo

University of California, San Diego, USA

L. Bauerdick, K. Burkett, I. Fisk, Y. Gao, O. Gutsche, B. Hooberman, S. Jindariani, J. Linacre, V. Martinez Otschoorn

Fermi National Accelerator Laboratory, Batavia, Illinois, USA

Abstract

This note describes a search for beyond-the-standard model (BSM) physics in events with a leptonically-decaying Z boson, jets, and missing transverse energy (E_T^{miss}). This signature is predicted to occur in several BSM scenarios, for example supersymmetric (SUSY) models. Two search strategies are pursued. The first is an inclusive approach which selects events with at least two jets and large E_T^{miss} , produced in association with the $Z \rightarrow \ell\ell$ candidate. The second is a targeted search in which additional requirements are imposed in order to achieve sensitivity to the production of the weakly-coupled SUSY charginos and neutralinos. The main backgrounds of SM $Z + \text{jets}$ and $t\bar{t}$ production are estimated with the data-driven E_T^{miss} templates technique and the opposite-flavor subtraction technique, respectively. Additional backgrounds are estimated from simulation after validation in data control samples. In the inclusive analysis, good agreement is observed between the data and predicted background over the full E_T^{miss} range. In the targeted analysis, good agreement is observed between the data and the predicted background in low E_T^{miss} control regions, which validates the background estimation methodology. The results in the signal regions of the targeted analysis, defined by the requirement $E_T^{\text{miss}} > 100$ GeV, will be unblinded soon after completion of signal optimization studies. These results will be interpreted in the context of simplified model spectra. The E_T^{miss} templates technique is also applied to the signal regions of the so-called “edge” analysis, as described in the appendices.

Contents

1	Changes w.r.t. previous AN Version	3
2	Introduction	3
3	Datasets and Triggers	5
4	Selection	6
4.1	Event Selection	6
4.2	Lepton Selection	6
4.2.1	Electron Selection	6
4.2.2	Muon Selection	6
4.3	Photons	6
4.4	MET	7
4.5	Jets	7
5	Data vs. MC Comparison in Preselection Region	8
6	Background Estimation Techniques	11
6.1	Estimating the Z + jets Background with E_T^{miss} Templates	11
6.2	Estimating the Flavor-Symmetric Background with $e\mu$ Events	12
6.3	Estimating the WZ and ZZ Background with MC	14
6.3.1	WZ Validation Studies	14
6.3.2	ZZ Validation Studies	16
7	Results	17
8	Interpretation	19
9	Summary	19
A	Results for the “edge analysis” SUS-12-019	21
A.1	Z Background Predictions for the “Edge Analysis”	21
B	Results in the ee and $\mu\mu$ Channels	28
C	E_T^{miss} Templates from γ + jets Sample	32

1 Changes w.r.t. previous AN Version

- v4: Update results of the low- E_T^{miss} and high- E_T^{miss} signal regions to 9.2 fb^{-1} , and un-blind the results of the inclusive analysis
- v3: Add results in the low- E_T^{miss} and high- E_T^{miss} signal regions used for the edge analysis for the first 5.1 fb^{-1} (see App. A).
- v2: Update to 9.2 fb^{-1} of 53X data and MC (v1 used 5.1 fb^{-1} 52X data and MC).

2 Introduction

This note presents two searches for beyond-the-standard model (BSM) physics in events containing a leptonically-decaying Z boson, jets, and missing transverse energy. This is an update of previous searches performed with 2011 data [1, 2]. The search is based on a data sample of pp collisions collected at $\sqrt{s} = 8 \text{ TeV}$ in 2012, corresponding to an integrated luminosity of 9.2 fb^{-1} . **For those readers interested in the “edge analysis” SUS-12-019, the relevant results may be found in App. A.**

The production of Z bosons is expected in many BSM scenarios, for example supersymmetric (SUSY) models. In SUSY models with neutralino lightest SUSY particle (LSP), Z bosons may be produced in the decays $\chi_2^0 \rightarrow Z\chi_1^0$, where χ_2^0 is the second lightest neutralino and χ_1^0 is the lightest neutralino. In models with gravitino LSP such as gauge-mediated SUSY breaking (GMSB) models, Z bosons may be produced via $\chi_1^0 \rightarrow Z\tilde{G}$, where \tilde{G} is the gravitino. Such decays may occur either in the cascade decays of the strongly-produced squarks and gluinos, or via direct production of the electroweak charginos and neutralino. Examples of such processes (see Fig. 1) are:

- strong production: $pp \rightarrow \tilde{g}\tilde{g} \rightarrow (q\bar{q}\chi_2^0)(q\bar{q}\chi_2^0) \rightarrow (q\bar{q}Z\chi_1^0)(q\bar{q}Z\chi_1^0) \rightarrow ZZ + 4 \text{ jets} + E_T^{\text{miss}}$
- electroweak production: $pp \rightarrow \chi_1^\pm \chi_2^0 \rightarrow (W\chi_1^0)(Z\chi_1^0) \rightarrow WZ + E_T^{\text{miss}}$

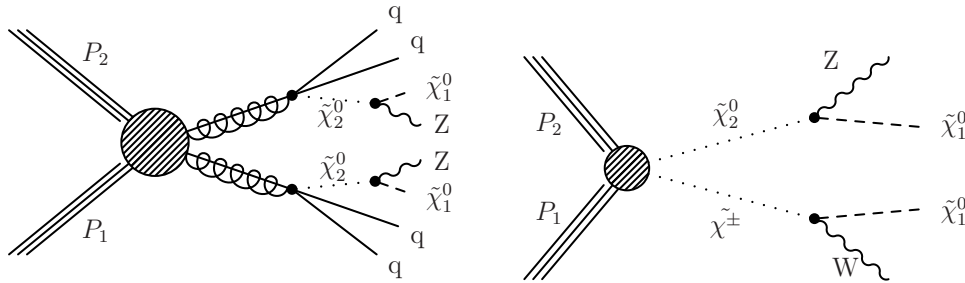


Figure 1: Examples of BSM physics signatures targeted in this search. In the left diagram, Z bosons are produced in the cascade decays of the strongly-interacting gluinos. In the right diagram, a Z boson is produced via direct production of the weakly-coupled charginos and neutralinos.

We thus pursue two strategies. The first is an inclusive strategy which selects events with a $Z \rightarrow \ell\ell$ candidate, at least two jets, and large E_T^{miss} . This strategy is useful for targeting, e.g., the production of Z bosons in the cascade decays of strongly-interacting particles as depicted in Fig. 1 (left). In the second strategy, we impose additional requirements which strongly suppress the backgrounds while retaining high efficiency for events with Z bosons produced via direct production of the weakly-coupled charginos and neutralinos. These two strategies are referred to as the “inclusive search” and the “targeted search,” respectively.

After selecting events with jets and a $Z \rightarrow \ell^+\ell^-$ ($\ell = e, \mu$) candidate, the dominant background consists of SM Z production accompanied by jets from initial-state radiation (Z + jets). The E_T^{miss} in Z + jets events arises primarily when jet energies are mismeasured. The Z + jets cross section is several orders of magnitude larger than our signal, and the artificial E_T^{miss} is not necessarily well reproduced in simulation. Therefore, the critical prerequisite to a discovery of BSM physics in the Z + jets + E_T^{miss} final state is to establish that a potential excess is not due to SM Z + jets production accompanied by artificial E_T^{miss} from jet mismeasurements. In this note, the Z + jets background is estimated with the E_T^{miss} templates technique, in which the artificial E_T^{miss} in Z + jets events is modeled using a γ + jets control sample. The second background category consists of processes which produce leptons with uncorrelated flavor. These “flavor-symmetric” (FS) backgrounds, which are dominated by $t\bar{t}$

³⁶ but also contain WW , $DY \rightarrow \tau\tau$ and single top processes, are estimated using a data control sample of $e\mu$ events.
³⁷ Additional backgrounds from WZ and ZZ production are estimated from MC, after validation of the MC modeling
³⁸ of these processes using 3-lepton and 4-lepton data control samples.

3 Datasets and Triggers

In this section we list the datasets, triggers, and MC samples used in the analysis. For selecting signal events, we use dilepton triggers in the DoubleElectron, DoubleMu, and MuEG datasets. An event in the ee final state is required to pass the dielectron trigger, a $\mu\mu$ event is required to pass the dimuon trigger, while an $e\mu$ event is required to pass at least one of the two $e - \mu$ cross triggers. The efficiencies of the ee , $\mu\mu$ and $e\mu$ triggers with respect to the offline selection have been measured as 0.95 ± 0.03 , 0.88 ± 0.03 , and 0.92 ± 0.03 , respectively [6]. These trigger efficiencies were measured with the first 5.1 fb^{-1} and will be updated with the full data sample. Preliminary measurements of the trigger efficiency with the full sample show consistent results within $\sim 1 - 2\%$. A sample of $\gamma + \text{jets}$ events, used as a control sample to estimate the $Z + \text{jets}$ background, is selected using a set of single photon triggers. The golden json of Aug 31st, corresponding to an integrated luminosity of 9.7 fb^{-1} , is used as the starting point. However, due to a bug in the Run2012C-PromptReco-v1 data samples (corresponding to 0.5 fb^{-1}), this portion of the data is currently excluded but will be added back after it is reprocessed. Thus we currently use a sample corresponding to 9.2 fb^{-1} . All data and MC samples are processed in CMSSW_5.3.2_patch4.

• Datasets

- /DoubleElectron/Run2012A-13Jul2012-v1/AOD
- /DoubleMu/Run2012A-13Jul2012-v1/AOD
- /MuEG/Run2012A-13Jul2012-v1/AOD
- /DoubleElectron/Run2012B-13Jul2012-v1/AOD
- /DoubleMu/Run2012B-13Jul2012-v1/AOD
- /MuEG/Run2012B-13Jul2012-v1/AOD
- /DoubleElectron/Run2012C-PromptReco-v2/AOD
- /DoubleMu/Run2012C-PromptReco-v2/AOD
- /MuEG/Run2012C-PromptReco-v2/AOD

• Triggers

- HLT_Mu17_Mu8_v*
- HLT_Mu17_Ele8_CaloIdT_CaloIsoVL_TrkIdVL_TrkIsoVL_v*
- HLT_Mu8_Ele17_CaloIdT_CaloIsoVL_TrkIdVL_TrkIsoVL*
- HLT_Ele17_CaloIdT_CaloIsoVL_TrkIdVL_TrkIsoVL_Ele8_CaloIdT_CaloIsoVL_TrkIdVL_TrkIsoVL_v*
- HLT_Photon22_R9Id90_HE10_Iso40_EBOnly_v*
- HLT_Photon36_R9Id90_HE10_Iso40_EBOnly_v*
- HLT_Photon50_R9Id90_HE10_Iso40_EBOnly_v*
- HLT_Photon75_R9Id90_HE10_Iso40_EBOnly_v*
- HLT_Photon90_R9Id90_HE10_Iso40_EBOnly_v*

Table 1: List of MC samples.

Process	Dataset Name	Cross Section [pb]
$Z + \text{jets}$	/DYJetsToLL_M-50_TuneZ2star_8TeV-madgraph-tarball/Summer12_DR53X-PU_S10_START53_V7A-v1/AODSIM	3532.8
$t\bar{t}$	/TTJets_MassiveBinDECAY_TuneZ2star_8TeV-madgraph-tauola/Summer12_DR53X-PU_S10_START53_V7A-v1/AODSIM	225.2
ZZ	/ZZJetsTo4L_TuneZ2star_8TeV-madgraph-tauola/Summer12_DR53X-PU_S10_START53_V7A-v1/AODSIM	0.1769
	/ZZJetsTo2L2Q_TuneZ2star_8TeV-madgraph-tauola/Summer12_DR53X-PU_S10_START53_V7A-v1/AODSIM	2.4487
	/ZZJetsTo2L2Nu_TuneZ2star_8TeV-madgraph-tauola/Summer12_DR53X-PU_S10_START53_V7A-v3/AODSIM	0.3648
WZ	/WZJetsTo3LNu_TuneZ2_8TeV-madgraph-tauola/Summer12_DR53X-PU_S10_START53_V7A-v1/AODSIM	1.0575
	/WZJetsTo2L2Q_TuneZ2star_8TeV-madgraph-tauola/Summer12_DR53X-PU_S10_START53_V7A-v1/AODSIM	2.206
WW	/WWJetsTo2L2Nu_TuneZ2star_8TeV-madgraph-tauola/Summer12_DR53X-PU_S10_START53_V7A-v1/AODSIM	5.8123
single top	/T_tW-channel-DR_TuneZ2star_8TeV-powheg-tauola/Summer12_DR53X-PU_S10_START53_V7A-v1/AODSIM	11.177
	/Tbar_tW-channel-DR_TuneZ2star_8TeV-powheg-tauola/Summer12_DR53X-PU_S10_START53_V7A-v1/AODSIM	11.177
$t\bar{t}V$	/TTZJets_8TeV-madgraph_v2/Summer12_DR53X-PU_S10_START53_V7A-v1/AODSIM	0.208
	/TTWJets_8TeV-madgraph/Summer12_DR53X-PU_S10_START53_V7A-v1/AODSIM	0.232
VVV	/ZZZNoGstarJets_8TeV-madgraph/Summer12_DR53X-PU_S10_START53_V7A-v1/AODSIM	0.01922
	/WWWJets_8TeV-madgraph/Summer12_DR53X-PU_S10_START53_V7A-v1/AODSIM	0.08217
	/WWZNoGstarJets_8TeV-madgraph/Summer12_DR53X-PU_S10_START53_V7A-v1/AODSIM	0.0633

4 Selection

In this section, we list the event selection, electron and muon objects selections, jets, E_T^{miss} , and b-tagging selections used in this analysis. These selections are based on those recommended by the relevant POG's.

4.1 Event Selection

We require the presence of at least one primary vertex satisfying the standard quality criteria; namely, vertex is not fake, $\text{ndf} \geq 4$, $\rho < 2$ cm, and $|z| < 24$ cm.

4.2 Lepton Selection

Because $Z \rightarrow \ell\ell$ ($\ell = e, \mu$) is a final state with very little background, we restrict ourselves to events in which the Z boson decays to electrons or muons only. Therefore opposite sign leptons passing the identification and isolation requirements described below are required in each event.

- $p_T > 20$ GeV and $|\eta| < 2.4$;
- Opposite-sign same-flavor (SF) ee and $\mu\mu$ lepton pairs (opposite-flavor (OF) $e\mu$ lepton pairs are retained in a control sample used to estimate the FS contribution);
- For SF events, the dilepton invariant mass is required to be consistent with the Z mass; namely $81 < m_{\ell\ell} < 101$ GeV.

4.2.1 Electron Selection

The electron selection is the loose working point recommended by the E/gamma POG, as documented at [3]. Electrons with $p_T > 20$ GeV and $|\eta| < 2.4$ are considered. We use PF-based isolation with a cone size of $\Delta R < 0.3$, using the effective area rho corrections documented at [4], and we require a relative isolation < 0.15 . Electrons in the transition region defined by $1.4442 < |\eta_{SC}| < 1.566$ are rejected. Electrons with a selected muon with $p_T > 10$ GeV within $\Delta R < 0.1$ are rejected. The electron selection requirements are listed in Table 2 for completeness.

Table 2: Summary of the electron selection requirements.

Quantity	Barrel	Endcap
$\delta\eta$	< 0.007	< 0.009
$\delta\phi$	< 0.15	< 0.10
$\sigma_{i\eta i\eta}$	< 0.01	< 0.03
H/E	< 0.12	< 0.10
d_0 (w.r.t. 1st good PV)	< 0.02 cm	< 0.02 cm
d_z (w.r.t. 1st good PV)	< 0.2 cm	< 0.2 cm
$ 1/E - 1/P $	$< 0.05 \text{ GeV}^{-1}$	$< 0.05 \text{ GeV}^{-1}$
PF isolation / p_T	< 0.15	< 0.15
conversion rejection: fit probability	$< 10^{-6}$	$< 10^{-6}$
conversion rejection: missing hits	≤ 1	≤ 1

4.2.2 Muon Selection

We use the tight muon selection recommended by the muon POG, as documented at [5]. Muons with $p_T > 20$ GeV and $|\eta| < 2.4$ are considered. We use PF-based isolation with a cone size of $\Delta R < 0.3$, using the $\Delta\beta$ PU correction scheme, and we require a relative isolation of < 0.15 . The muon selection requirements are listed in Table 3 for completeness.

4.3 Photons

As will be explained later, it is not essential that we select real photons. What is needed are jets that are predominantly electromagnetic, well measured in the ECAL, and hence less likely to contribute to fake MET. We select photons with:

Table 3: Summary of the muons selection requirements.

Quantity	Requirement
muon type	global muon and PF muon
χ^2/ndf	< 10
muon chamber hits	≥ 1
matched stations	≥ 2
d_0 (w.r.t. 1st good PV)	$< 0.02 \text{ cm}$
d_z (w.r.t. 1st good PV)	$< 0.5 \text{ cm}$
pixel hits	≥ 1
tracker layers	≥ 5

- $p_T > 22 \text{ GeV}$
- $|\eta| < 2$
- $H/E < 0.1$
- No matching pixel track (pixel veto)
- There must be a pfjet of $p_T > 10 \text{ GeV}$ matched to the photon within $dR < 0.3$. The matched jet is required to have a neutral electromagnetic energy fraction of at least 70%.
- We require that the pfjet p_T matched to the photon satisfy (pfjet p_T - photon p_T) $> -5 \text{ GeV}$. This removes a few rare cases in which “overcleaning” of a pfjet generates fake MET.
- We also match photons to calojets and require (calojet p_T - photon p_T) $> -5 \text{ GeV}$ (the same requirement used for pfjets). This is to remove other rare cases in which fake energy is added to the photon object but not the calojet.
- We reject photons which have an electron of at least $p_T > 10 \text{ GeV}$ within $dR < 0.2$ in order to reject conversions from electrons from W decays which are accompanied by real MET.
- We reject photons which are aligned with the MET to within 0.14 radians in phi.

4.4 MET

We use pfmet, henceforth referred to simply as E_T^{miss} .

4.5 Jets

- PF jets with L1FastL2L3 corrections (MC), L1FastL2L3residual corrections (data), using the 52X jet energy corrections
- $|\eta| < 2.5$
- Passes loose PFJet ID
- $p_T > 30 \text{ GeV}$ for determining the jet multiplicity, $p_T > 15 \text{ GeV}$ for calculation of H_T
- For the creation of photon templates, the jet matched to the photon passing the photon selection described above is vetoed
- For the dilepton sample, jets are vetoed if they are within $\Delta R < 0.4$ from any lepton $p_T > 20 \text{ GeV}$ passing analysis selection

5 Data vs. MC Comparison in Preselection Region

In this section we compare the data and MC samples passing the selection described in Sec. 4. In the following, the MC is reweighted to match the data distribution of number of reconstructed primary vertices. The trigger efficiencies of Sec. 3 are applied. In all plots, the last bin contains the overflow.

We begin by counting the inclusive Z yields. Here we require the presence of two selected leptons without any additional requirements on jets or E_T^{miss} . In Fig. 2 the distribution of dilepton invariant mass in the ee and $\mu\mu$ channels is displayed. In Table 4 the yields for selected dilepton events in the Z mass window are indicated. Good data vs. MC agreement is observed, within the systematic uncertainties of integrated luminosity (4.5%), trigger efficiency (3%), Z + jets and $t\bar{t}$ cross sections.

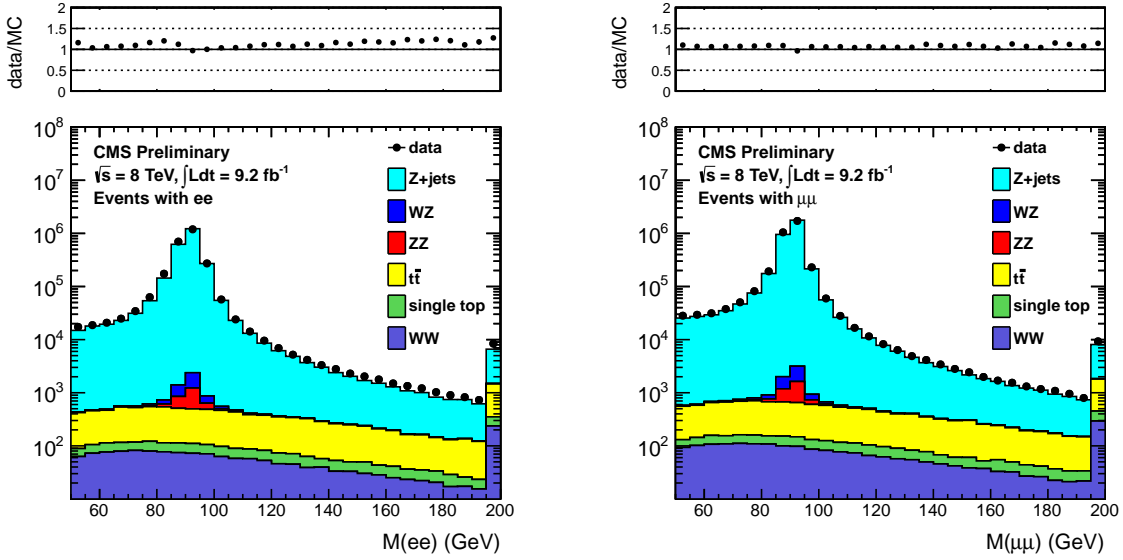


Figure 2: Dilepton mass distribution for events with two selected leptons in the ee (left) and $\mu\mu$ (right) final states.

Table 4: Data and Monte Carlo yields for events with two selected leptons in the Z mass window.

Sample	ee	$\mu\mu$	$e\mu$	total
Z + jets	22662501 ± 1660	3125059 ± 1873	1082 ± 35.8	5392392 ± 2503
$t\bar{t}$	1579.1 ± 22.6	1998.3 ± 24.4	3592.2 ± 33.5	7169.5 ± 47.2
WW	290.6 ± 2.9	387.2 ± 3.3	671.2 ± 4.4	1349.0 ± 6.2
WZ	2052.6 ± 3.6	2686.9 ± 3.9	54.1 ± 0.5	4793.5 ± 5.3
ZZ	1294.6 ± 2.7	1708.5 ± 3.0	5.2 ± 0.1	3008.3 ± 4.0
single top	150.0 ± 5.9	192.6 ± 6.4	332.9 ± 8.6	675.5 ± 12.2
total SM MC	2271617 ± 1661	3132032 ± 18723	5738 ± 50.0	5409387 ± 2503
data	2329993	3169480	6182	5505655

We next define the preselection region for the inclusive search using the following requirements:

- Number of jets ≥ 2 ;
- Same flavor dileptons (opposite flavor yields will be shown since they are used in data for the FS background estimation);
- Dilepton invariant mass $81 < m_{\ell\ell} < 101$ GeV.

The dilepton mass distributions in the preselection region of the inclusive search (without the dilepton mass requirement applied) for the ee and $\mu\mu$ final states are shown in Figure 3. In Table 5 the data and MC yields in the preselection region are indicated. Good data vs. MC agreement is observed.

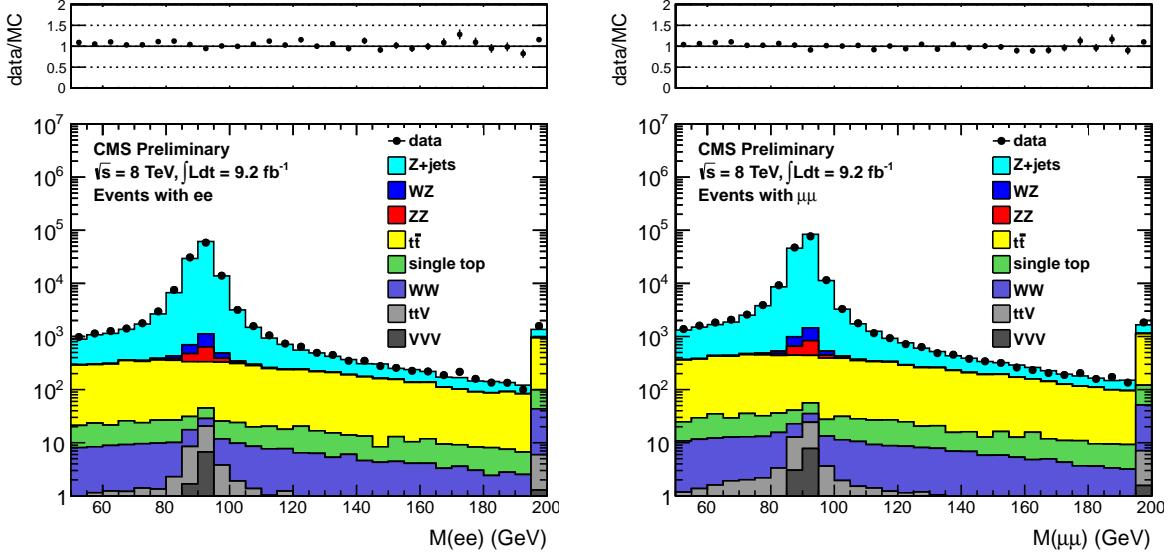


Figure 3: Dilepton mass distribution for events in the preselection region of the inclusive search in the ee (left) and $\mu\mu$ (right) final states.

Table 5: Data and MC yields in the preselection region of the inclusive search.

Sample	ee	$\mu\mu$	$e\mu$	total
Z + jets	108778.2 ± 358.0	145999.4 ± 398.7	59.7 ± 8.3	254837.4 ± 535.9
$t\bar{t}$	1220.9 ± 19.9	1544.7 ± 21.4	2788.1 ± 29.5	5553.8 ± 41.5
WW	32.7 ± 1.0	42.5 ± 1.1	74.7 ± 1.4	149.9 ± 2.0
WZ	853.0 ± 2.4	1100.8 ± 2.6	10.7 ± 0.2	1964.4 ± 3.5
ZZ	532.5 ± 1.8	692.6 ± 2.0	1.2 ± 0.0	1226.3 ± 2.7
single top	60.4 ± 3.7	73.1 ± 3.9	131.8 ± 5.4	265.3 ± 7.6
ttV	25.9 ± 0.5	32.2 ± 0.5	9.4 ± 0.3	67.5 ± 0.8
VVV	9.2 ± 0.1	11.6 ± 0.2	1.6 ± 0.1	22.5 ± 0.2
tot SM MC	111512.9 ± 358.6	149497.0 ± 399.3	3077.2 ± 31.1	264087.1 ± 537.6
data	110325	144122	2966	257413

We next define the preselection region for the targeted search by adding the following requirements:

- Veto events containing a b-tagged jet;
- Dijet invariant mass $70 < m_{jj} < 110$ GeV;
- Veto events containing a third selected lepton (electron or muon) with $p_T > 10$ GeV;

The rejection of events with a b-tagged jet strongly suppresses the $t\bar{t}$ background, which is the dominant background in the inclusive search after requiring large E_T^{miss} . The requirement that the jet pair is consistent with originating from W/Z decay is motivated by the fact that we are searching for signatures producing $V(jj)Z(\ell\ell)+E_T^{\text{miss}}$; this requirement suppresses the $Z + \text{jets}$ and $t\bar{t}$ backgrounds. The veto of events containing a third electron or muon suppresses the WZ background, and also serves to make this analysis exclusive with respect to searches in the trilepton final state.

The dilepton mass distributions in the preselection region of the targeted search (without the dilepton mass requirement applied) for the ee and $\mu\mu$ final states are shown in Figure 4. In Table 6 the data and MC yields in the preselection region are indicated. Good data vs. MC agreement is observed. We also show the distribution of dijet mass in the targeted preselection (with the requirement on this quantity removed) in Fig. 5, which demonstrates that the MC does a reasonable job of modeling this quantity.

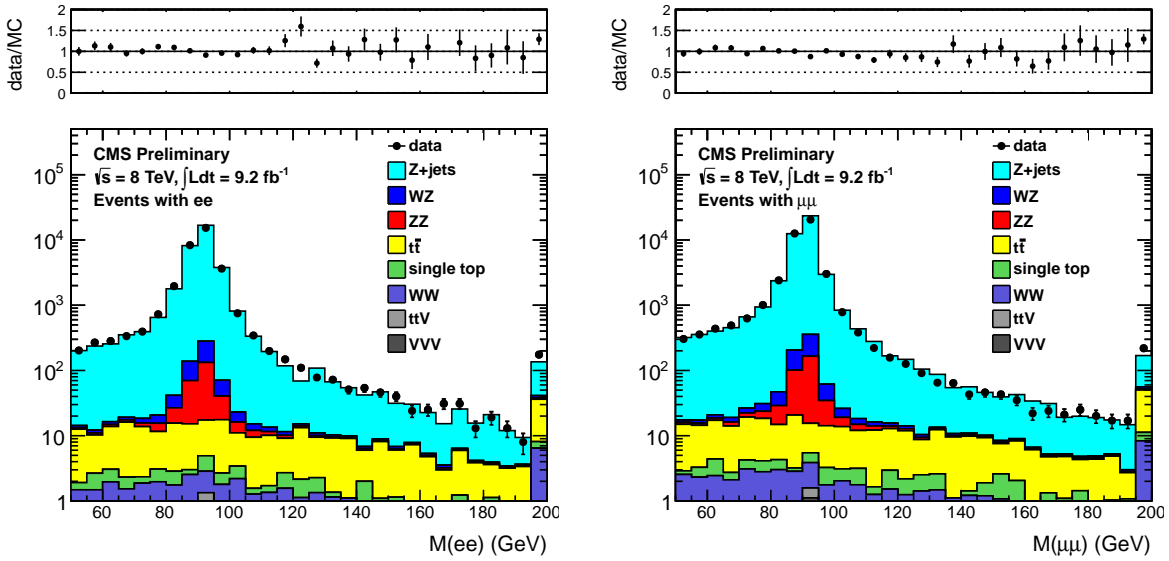


Figure 4: Dilepton mass distribution for events in the preselection region of the targeted search in the ee (left) and $\mu\mu$ (right) final states.

Table 6: Data and MC yields in the preselection region of the targeted search.

Sample	ee	$\mu\mu$	$e\mu$	total
Z + jets	30033.0 ± 186.9	40552.4 ± 208.9	12.9 ± 3.7	70598.3 ± 280.4
$t\bar{t}$	50.5 ± 4.1	49.1 ± 3.8	105.1 ± 5.7	204.7 ± 8.0
WW	6.8 ± 0.4	8.6 ± 0.5	15.9 ± 0.7	31.3 ± 0.9
WZ	260.7 ± 1.3	339.8 ± 1.4	1.7 ± 0.1	602.2 ± 2.0
ZZ	204.2 ± 1.1	264.0 ± 1.2	0.2 ± 0.0	468.4 ± 1.7
single top	4.7 ± 1.1	5.0 ± 1.0	8.5 ± 1.3	18.2 ± 2.0
ttV	0.7 ± 0.1	0.8 ± 0.1	0.4 ± 0.1	2.0 ± 0.1
VVV	1.4 ± 0.1	1.8 ± 0.1	0.4 ± 0.0	3.6 ± 0.1
tot SM MC	30562.0 ± 187.0	41221.5 ± 208.9	145.2 ± 7.0	71928.6 ± 280.5
data	29183	38388	120	67691

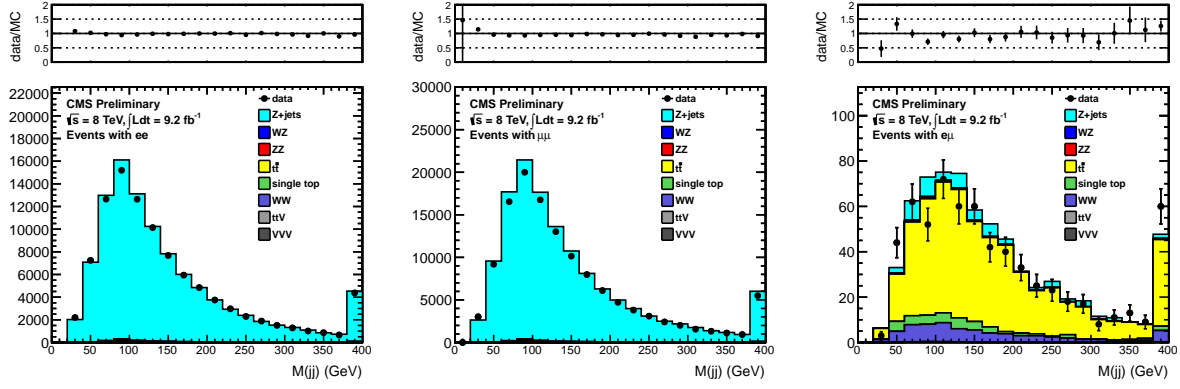


Figure 5: Distributions of dijet mass for the targeted preselection in the ee (left), $\mu\mu$ (middle) and $e\mu$ (right) final state.

6 Background Estimation Techniques

In this section we describe the techniques used to estimate the SM backgrounds in our signal regions defined by requirements of large E_T^{miss} . The SM backgrounds fall into three categories:

- $Z + \text{jets}$: this is the dominant background after the preselection. The E_T^{miss} in $Z + \text{jets}$ events is estimated with the “ E_T^{miss} templates” technique described in Sec. 6.1;
- Flavor-symmetric (FS) backgrounds: this category includes processes which produces 2 leptons of uncorrelated flavor. It is dominated by $t\bar{t}$ but also contains $Z \rightarrow \tau\tau$, WW , and single top processes. This is the dominant contribution in the signal regions, and it is estimated using a data control sample of $e\mu$ events as described in Sec. 6.2;
- WZ and ZZ backgrounds: this background is estimated from MC, after validating the MC modeling of these processes using data control samples with jets and exactly 3 leptons (WZ control sample) and exactly 4 leptons (ZZ control sample) as described in Sec. 6.3;

6.1 Estimating the $Z + \text{jets}$ Background with E_T^{miss} Templates

The premise of this data driven technique is that E_T^{miss} in $Z + \text{jets}$ events is produced by the hadronic recoil system and *not* by the leptons making up the Z . Therefore, the basic idea of the E_T^{miss} template method is to measure the E_T^{miss} distribution in a control sample which has no true MET and the same general attributes regarding fake MET as in $Z + \text{jets}$ events. We thus use a sample of $\gamma + \text{jets}$ events, since both $Z + \text{jets}$ and $\gamma + \text{jets}$ events consist of a well-measured object recoiling against hadronic jets.

For selecting photon-like objects, the very loose photon selection described in Sec. 4.3 is used. It is not essential for the photon sample to have high purity. For our purposes, selecting jets with predominantly electromagnetic energy deposition in a good fiducial volume suffices to ensure that they are well measured and do not contribute to fake E_T^{miss} . The $\gamma + \text{jets}$ events are selected with a suite of single photon triggers with p_T thresholds varying from 22–90 GeV. The events are weighted by the trigger prescale such that $\gamma + \text{jets}$ events evenly sample the conditions over the full period of data taking. There remains a small difference in the PU conditions in the $\gamma + \text{jets}$ vs. $Z + \text{jets}$ samples due to the different dependencies of the γ vs. Z isolation efficiencies on PU. To account for this, we reweight the $\gamma + \text{jets}$ samples to match the distribution of reconstructed primary vertices in the $Z + \text{jets}$ sample.

To account for kinematic differences between the hadronic systems in the control vs. signal samples, we measure the E_T^{miss} distributions in the $\gamma + \text{jets}$ sample in bins of the number of jets and the scalar sum of jet transverse energies (H_T). These E_T^{miss} templates are extracted separately from the 5 single photon triggers with thresholds 22, 36, 50, 75, and 90 GeV, so that the templates are effectively binned in photon p_T . All E_T^{miss} distributions are normalized to unit area to form “MET templates”. The prediction of the MET in each Z event is the template which corresponds to the N_{jets} , H_T , and $Z p_T$ in the $Z + \text{jets}$ event. The prediction for the Z sample is simply the sum of all such templates. All templates are displayed in App. C.

After preselection, there is a small contribution from backgrounds other than $Z + \text{jets}$. To correct for this, the E_T^{miss} templates prediction is scaled such that the total background prediction matches the observed data yield in the E_T^{miss} 0–60 GeV region. Because the non- $Z + \text{jets}$ impurity in the low E_T^{miss} region after preselection is very small, this results in scaling factors of 0.985 (0.995) for the inclusive (targeted) search.

6.2 Estimating the Flavor-Symmetric Background with $e\mu$ Events

In this subsection we describe the background estimate for the FS background. Since this background produces equal rates of same-flavor (SF) ee and $\mu\mu$ lepton pairs as opposite-flavor (OF) $e\mu$ lepton pairs, the OF yield can be used to estimate the SF yield, after correcting for the different electron vs. muon offline selection efficiencies and the different efficiencies for the ee , $\mu\mu$, and $e\mu$ triggers.

An important quantity needed to translate from the OF yield to a prediction for the background in the SF final state is the ratio $R_{\mu e} = \epsilon_\mu / \epsilon_e$, where ϵ_μ (ϵ_e) indicates the offline muon (electron) selection efficiency. This quantity can be extracted from data using the observed $Z \rightarrow \mu\mu$ and $Z \rightarrow ee$ yields in the preselection region, after correcting for the different trigger efficiencies.

Hence we define:

- $N_{ee}^{\text{trig}} = \epsilon_{ee}^{\text{trig}} N_{ee}^{\text{offline}}$,
- $N_{\mu\mu}^{\text{trig}} = \epsilon_{\mu\mu}^{\text{trig}} N_{\mu\mu}^{\text{offline}}$,
- $N_{e\mu}^{\text{trig}} = \epsilon_{e\mu}^{\text{trig}} N_{e\mu}^{\text{offline}}$.

Here $N_{\ell\ell}^{\text{trig}}$ denotes the number of selected Z events in the $\ell\ell$ channel passing the offline and trigger selection (in other words, the number of recorded and selected events), $\epsilon_{\ell\ell}^{\text{trig}}$ is the trigger efficiency, and $N_{\ell\ell}^{\text{offline}}$ is the number of events that would have passed the offline selection if the trigger had an efficiency of 100%. Thus we calculate the quantity:

$$R_{\mu e} = \sqrt{\frac{N_{\mu\mu}^{\text{offline}}}{N_{ee}^{\text{offline}}}} = \sqrt{\frac{N_{\mu\mu}^{\text{trig}} / \epsilon_{\mu\mu}^{\text{trig}}}{N_{ee}^{\text{trig}} / \epsilon_{ee}^{\text{trig}}}} = \sqrt{\frac{144122/0.88}{110325/0.95}} = 1.19 \pm 0.07. \quad (1)$$

Here we have used the $Z \rightarrow \mu\mu$ and $Z \rightarrow ee$ yields from Table 5 and the trigger efficiencies quoted in Sec. 3. The indicated uncertainty is due to the 3% uncertainties in the trigger efficiencies. The predicted yields in the ee and $\mu\mu$ final states are calculated from the observed $e\mu$ yield as

- $N_{ee}^{\text{predicted}} = \frac{N_{e\mu}^{\text{trig}} \epsilon_{ee}^{\text{trig}}}{\epsilon_{e\mu}^{\text{trig}} 2 R_{\mu e}} = \frac{N_{e\mu}^{\text{trig}} 0.95}{0.92 \cdot 2 \times 1.26} = (0.43 \pm 0.05) \times N_{e\mu}^{\text{trig}}$,
- $N_{\mu\mu}^{\text{predicted}} = \frac{N_{e\mu}^{\text{trig}} \epsilon_{\mu\mu}^{\text{trig}} R_{\mu e}}{\epsilon_{e\mu}^{\text{trig}} 2} = \frac{N_{e\mu}^{\text{trig}} 0.88 \times 1.26}{0.95 \cdot 2} = (0.55 \pm 0.07) \times N_{e\mu}^{\text{trig}}$,

and the predicted yield in the combined ee and $\mu\mu$ channel is simply the sum of these two predictions:

- $N_{ee+\mu\mu}^{\text{predicted}} = (0.99 \pm 0.06) \times N_{e\mu}^{\text{trig}}$.

Note that the relative uncertainty in the combined ee and $\mu\mu$ prediction is smaller than those for the individual ee and $\mu\mu$ predictions because the uncertainty in $R_{\mu e}$ cancels when summing the ee and $\mu\mu$ predictions.

To improve the statistical precision of the FS background estimate, we remove the requirement that the $e\mu$ lepton pair falls in the Z mass window. Instead we scale the $e\mu$ yield by K , the efficiency for $e\mu$ events to satisfy the Z mass requirement, extracted from simulation. In Fig. 6 we display the value of K in data and simulation, for a variety of E_T^{miss} requirements, for the inclusive analysis. Based on this we chose $K = 0.14 \pm 0.02$ for the lower E_T^{miss} regions, $K = 0.14 \pm 0.04$ for the $E_T^{\text{miss}} > 200$ GeV region, and $K = 0.14 \pm 0.09$ for $E_T^{\text{miss}} > 300$ GeV, where the larger uncertainties reflect the reduced statistical precision at large E_T^{miss} . The corresponding plot for the targeted analysis, including the b-veto, is displayed in Fig. 7. Based on this we chose $K = 0.13 \pm 0.02$ for all E_T^{miss} regions up to $E_T^{\text{miss}} > 150$ GeV. For the $E_T^{\text{miss}} > 200$ GeV region we choose $K = 0.13 \pm 0.05$, due to the reduced statistical precision.

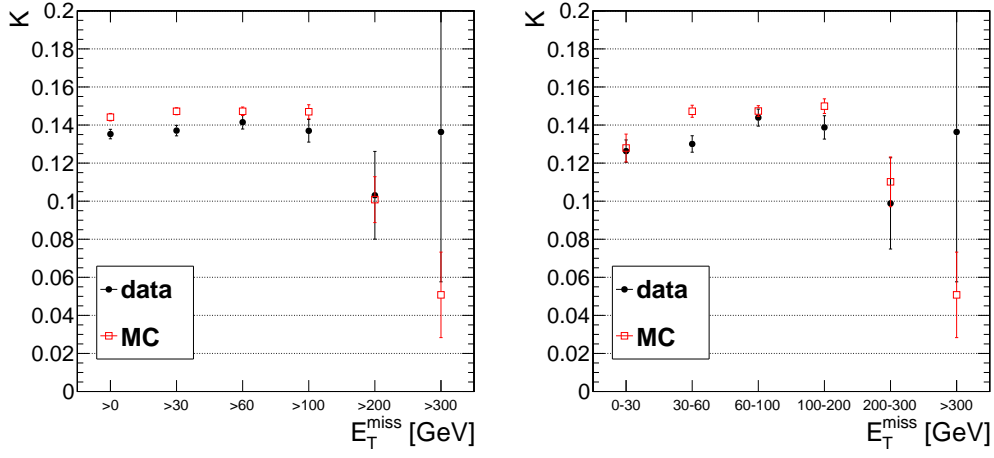


Figure 6: The efficiency for $e\mu$ events to satisfy the dilepton mass requirement, K , in data and simulation for inclusive E_T^{miss} intervals (left) and exclusive E_T^{miss} intervals (right) for the inclusive analysis.

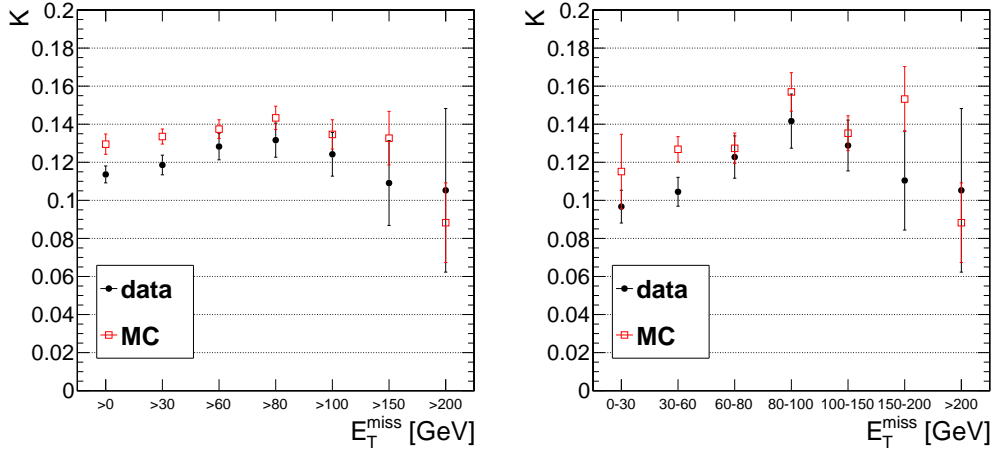


Figure 7: The efficiency for $e\mu$ events to satisfy the dilepton mass requirement, K , in data and simulation for inclusive E_T^{miss} intervals (left) and exclusive E_T^{miss} intervals (right) for the targeted analysis, including the b-veto. Based on this we chose $K = 0.13 \pm 0.02$ for the E_T^{miss} regions up to $E_T^{\text{miss}} > 100$ GeV. For higher E_T^{miss} regions we chose $K = 0.13 \pm 0.07$.

6.3 Estimating the WZ and ZZ Background with MC

Backgrounds from $W(\ell\nu)Z(\ell\ell)$ where the W lepton is not identified or is outside acceptance, and $Z(\nu\nu)Z(\ell\ell)$, are estimated from simulation. The MC modeling of these processes is validated by comparing the MC predictions with data in control samples with exactly 3 leptons (WZ control sample) and exactly 4 leptons (ZZ control sample). The critical samples are the WZJetsTo3LNu and ZZJetsTo4L, listed in Table 1 (the WZJetsTo2L2Q, ZZJetsTo2L2Q, and ZZJetsTo2L2Nu samples are also used in this analysis but their contribution to the 3-lepton and 4-lepton control samples is negligible).

6.3.1 WZ Validation Studies

A pure WZ sample can be selected in data with the requirements:

- Exactly 3 $p_T > 20$ GeV leptons passing analysis identification and isolation requirements,
- 2 of the 3 leptons must fall in the Z window 81-101 GeV,
- $E_T^{\text{miss}} > 50$ GeV (to suppress DY).

The data and MC yields passing the above selection are in Table 7. The inclusive yields (without any jet requirements) agree within 13%, which is consistent within the uncertainty in the CMS measured WZ cross section (17%). A data vs. MC comparison of kinematic distributions (jet multiplicity, E_T^{miss} , $Z p_T$) is given in Fig. 8. High E_T^{miss} values in WZ and ZZ events arise from highly boosted W or Z bosons that decay leptonically, and we therefore check that the MC does a reasonable job of reproducing the p_T distributions of the leptonically decaying Z. While the inclusive WZ yields are in reasonable agreement, we observe an excess in data in events with at least 2 jets, corresponding to the jet multiplicity requirement in our preselection. We observe 106 events in data while the MC predicts 62 ± 1.5 (stat), representing an excess of 71%, as indicated in Table 8. This excess will be studied further. For the time being, based on these studies we currently assess an uncertainty of 70% on the WZ yield.

Table 7: Data and Monte Carlo yields passing the WZ preselection.

Sample	ee	$\mu\mu$	$e\mu$	total
WZ	116.7 ± 0.8	151.5 ± 0.8	8.1 ± 0.2	276.3 ± 1.2
ttV	4.1 ± 0.2	4.9 ± 0.2	1.2 ± 0.1	10.2 ± 0.3
$t\bar{t}$	1.2 ± 0.6	3.2 ± 0.9	3.6 ± 1.0	7.9 ± 1.5
ZZ	2.5 ± 0.0	3.4 ± 0.0	0.2 ± 0.0	6.1 ± 0.0
Z + jets	1.2 ± 0.9	3.0 ± 1.8	0.0 ± 0.0	4.2 ± 2.1
vvv	1.6 ± 0.1	2.1 ± 0.1	0.3 ± 0.0	4.0 ± 0.1
single top	0.0 ± 0.0	0.2 ± 0.2	0.0 ± 0.0	0.2 ± 0.2
WW	0.0 ± 0.0	0.0 ± 0.0	0.1 ± 0.0	0.1 ± 0.1
tot SM MC	127.3 ± 1.4	168.4 ± 2.3	13.5 ± 1.0	309.2 ± 2.8
data	156	178	16	350

Table 8: Data and Monte Carlo yields passing the WZ preselection and $N_{\text{jets}} \geq 2$.

Sample	ee	$\mu\mu$	$e\mu$	total
WZ	19.1 ± 0.3	24.6 ± 0.3	1.3 ± 0.1	44.9 ± 0.5
ttV	3.8 ± 0.2	4.5 ± 0.2	1.0 ± 0.1	9.3 ± 0.3
$t\bar{t}$	0.8 ± 0.5	1.6 ± 0.7	0.9 ± 0.5	3.3 ± 1.0
ZZ	0.5 ± 0.0	0.7 ± 0.0	0.0 ± 0.0	1.2 ± 0.0
Z + jets	0.9 ± 0.9	0.0 ± 0.0	0.0 ± 0.0	0.9 ± 0.9
vvv	0.9 ± 0.0	1.2 ± 0.1	0.1 ± 0.0	2.2 ± 0.1
single top	0.0 ± 0.0	0.2 ± 0.2	0.0 ± 0.0	0.2 ± 0.2
WW	0.0 ± 0.0	0.0 ± 0.0	0.0 ± 0.0	0.0 ± 0.0
tot SM MC	25.9 ± 1.1	32.9 ± 0.8	3.3 ± 0.5	62.1 ± 1.5
data	47	51	8	106

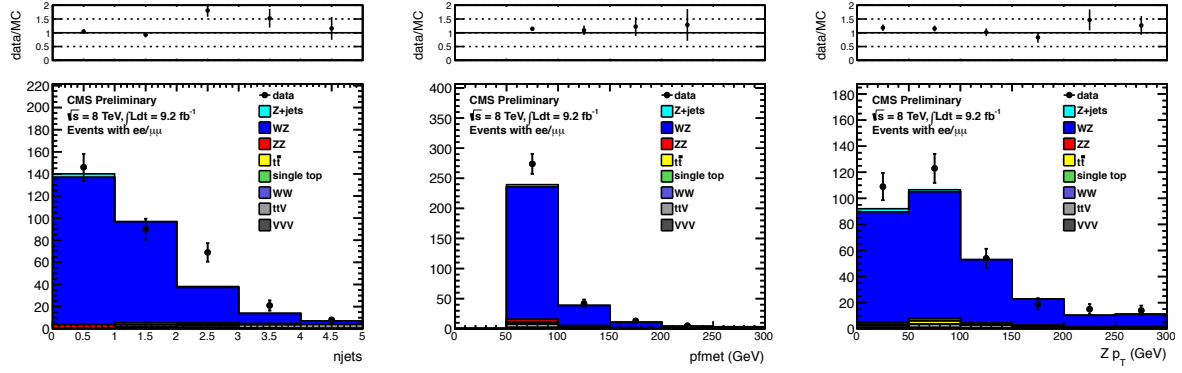


Figure 8: Data vs. MC comparisons for the WZ selection discussed in the text for 9.2 fb^{-1} . The number of jets, missing transverse energy, and Z boson transverse momentum are displayed.

6.3.2 ZZ Validation Studies

A pure ZZ sample can be selected in data with the requirements:

- Exactly 4 $p_T > 20$ GeV leptons passing analysis identification and isolation requirements,
- 2 of the 4 leptons must fall in the Z window 81-101 GeV.

The data and MC yields passing the above selection are in Table 9. In this ZZ-dominated sample we observe good agreement between the data yield and the MC prediction. After requiring 2 jets (corresponding to the requirement in the analysis selection), we observe 4 events in data and the MC predicts 6.6 ± 0.1 events. Due to the limited statistical precision we assign an uncertainty of 50% on the ZZ yield.

Table 9: Data and Monte Carlo yields for the ZZ preselection.

Sample	ee	$\mu\mu$	$e\mu$	total
ZZ	25.1 ± 0.1	34.9 ± 0.1	1.6 ± 0.0	61.7 ± 0.1
ttV	0.6 ± 0.1	0.6 ± 0.1	0.2 ± 0.0	1.4 ± 0.1
VVV	0.3 ± 0.0	0.4 ± 0.0	0.0 ± 0.0	0.7 ± 0.0
WZ	0.1 ± 0.0	0.1 ± 0.0	0.0 ± 0.0	0.1 ± 0.0
Z + jets	0.0 ± 0.0	0.0 ± 0.0	0.0 ± 0.0	0.0 ± 0.0
$t\bar{t}$	0.0 ± 0.0	0.0 ± 0.0	0.0 ± 0.0	0.0 ± 0.0
single top	0.0 ± 0.0	0.0 ± 0.0	0.0 ± 0.0	0.0 ± 0.0
WW	0.0 ± 0.0	0.0 ± 0.0	0.0 ± 0.0	0.0 ± 0.0
tot SM MC	26.1 ± 0.1	36.1 ± 0.1	1.8 ± 0.0	63.9 ± 0.2
data	24	36	0	60

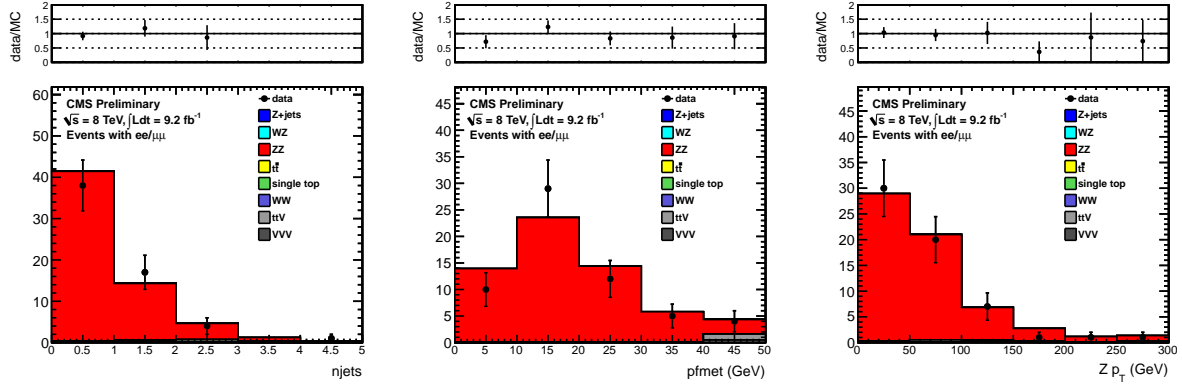


Figure 9: Data vs. MC comparisons for the ZZ selection discussed in the text for 9.2 fb^{-1} . The number of jets, missing transverse energy, and Z boson transverse momentum are displayed.

7 Results

In this section we provide the results of the inclusive and targeted searches. The observed and predicted E_T^{miss} distributions for the inclusive analysis are indicated in Fig. 10. A summary of the results in the signal regions is provided in Table 10. Currently we blind the observed data yields for the signal regions, defined by $E_T^{\text{miss}} > 100$ GeV. These yields will be presented when the decision is made to unblind the Z region for the Aachen/ETH low-mass opposite-sign same-flavor dilepton analysis (“edge analysis”). In the low E_T^{miss} region, we observe good agreement between the data and the predicted background, which validates the background estimation methodology. The separate results for the ee and $\mu\mu$ channels are presented in App. B.

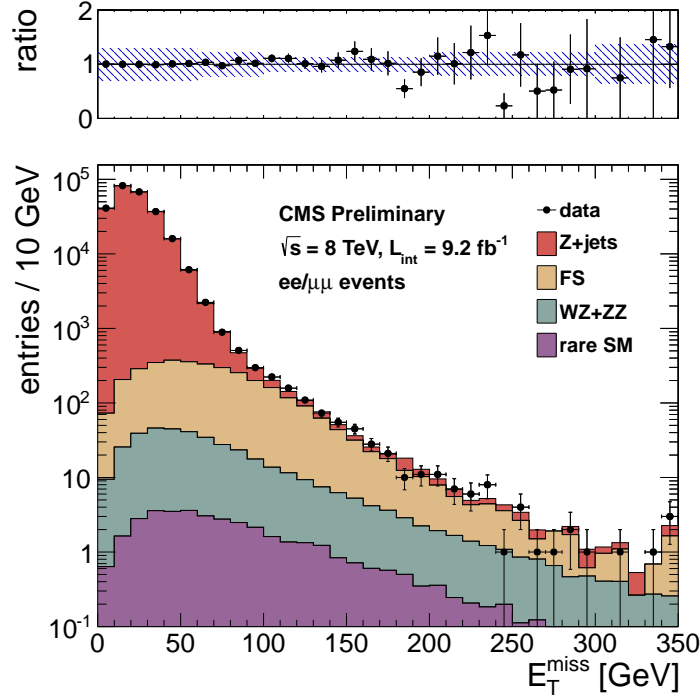


Figure 10: Results of the inclusive analysis. The observed E_T^{miss} distribution (black points) is compared with the sum of the predicted E_T^{miss} distributions from Z + jets , flavor-symmetric backgrounds, and WZ+ZZ backgrounds. The ratio of observed to predicted yields in each bin is indicated. The error bars indicate the statistical uncertainty in the data and the shaded band indicates the total background uncertainty.

Table 10: Summary of results in the inclusive analysis. The total background is the sum of the Z + jets background predicted from the E_T^{miss} templates method (Z + jets bkg), the flavor-symmetric background predicted from $e\mu$ events (FS bkg), and the WZ and ZZ backgrounds predicted from MC (WZ bkg and ZZ bkg). All uncertainties include both the statistical and systematic components. The Gaussian significance of the deviation between the data and total background is indicated for signal regions with at least 20 observed events.

	E_T^{miss} 0–30 GeV	E_T^{miss} 30–60 GeV	E_T^{miss} 60–100 GeV	E_T^{miss} 100–200 GeV	E_T^{miss} 200–300 GeV	$E_T^{\text{miss}} > 300$ GeV
Z + jets bkg	190111 ± 57034	57989 ± 17398	2744 ± 824	123 ± 37	7.4 ± 2.4	1.3 ± 0.5
FS bkg	492 ± 77	947 ± 147	981 ± 152	503 ± 78	23.6 ± 7.1	3.0 ± 1.9
WZ bkg	61.5 ± 43.0	104.8 ± 73.4	75.4 ± 52.8	41.2 ± 28.8	5.6 ± 3.9	1.6 ± 1.6
ZZ bkg	7.6 ± 3.8	16.2 ± 8.1	17.4 ± 8.7	16.1 ± 8.1	3.2 ± 1.6	1.0 ± 1.0
rare SM bkg	5.1 ± 2.5	10.7 ± 5.4	10.4 ± 5.2	9.1 ± 4.6	1.7 ± 0.8	0.6 ± 0.6
total bkg	190678 ± 57034	59068 ± 17398	3829 ± 840	692 ± 92	41.5 ± 8.7	7.5 ± 2.7
data	190793	58953	3921	733	42	5
significance	0.0σ	-0.0σ	0.1σ	0.4σ	0.0σ	

271 The observed and predicted E_T^{miss} distributions for the targeted analysis are indicated in Fig. 11. A summary of
 272 the results in the signal regions is provided in Table 11. The observed yields are in good agreement with the
 273 predicted background the low E_T^{miss} region, validating the background estimation methodology. In the signal
 274 regions defined by requirements of large E_T^{miss} , good agreement is found between the observed yields and the
 275 predicted background.

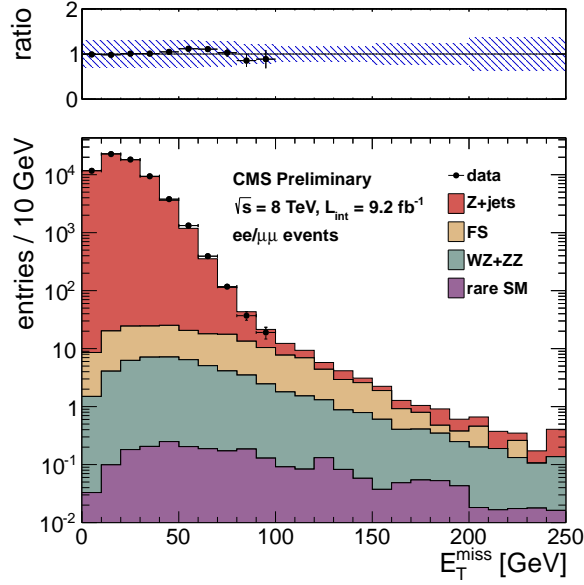


Figure 11: Results of the targeted analysis. The observed E_T^{miss} distribution (black points) is compared with the sum of the predicted E_T^{miss} distributions from Z + jets , flavor-symmetric backgrounds, and WZ+ZZ backgrounds. The ratio of observed to predicted yields in each bin is indicated. The error bars indicate the statistical uncertainty in the data and the shaded band indicates the total background uncertainty.

Table 11: Summary of results in the targeted analysis. The total background is the sum of the Z + jets background predicted from the E_T^{miss} templates method (Z + jets bkg), the flavor-symmetric background predicted from $e\mu$ events (FS bkg), and the WZ and ZZ backgrounds predicted from MC (WZ bkg and ZZ bkg). All uncertainties include both the statistical and systematic components. The Gaussian significance of the deviation between the data and total background is indicated for signal regions with at least 20 observed events.

	E_T^{miss} 0–30 GeV	E_T^{miss} 30–60 GeV	E_T^{miss} 60–80 GeV	E_T^{miss} 80–100 GeV
Z + jets bkg	52823 ± 15847	14015 ± 4205	433 ± 130	40.9 ± 12.4
FS bkg	41.3 ± 7.2	49.5 ± 8.6	26.4 ± 4.7	17.9 ± 3.3
WZ bkg	9.5 ± 6.6	15.9 ± 11.2	6.6 ± 4.7	3.9 ± 2.7
ZZ bkg	2.1 ± 1.0	4.1 ± 2.1	2.2 ± 1.1	1.8 ± 0.9
rare SM bkg	0.3 ± 0.2	0.7 ± 0.3	0.4 ± 0.2	0.3 ± 0.2
total bkg	52876 ± 15847	14085 ± 4205	468 ± 130	64.7 ± 13.2
data	52485	14476	510	56
significance	-0.0σ	0.1σ	0.3σ	-0.6σ
	E_T^{miss} 100–120 GeV	E_T^{miss} 120–150 GeV	E_T^{miss} 150–200 GeV	E_T^{miss} > 200 GeV
Z + jets bkg	7.0 ± 2.2	3.1 ± 0.9	1.6 ± 0.5	0.8 ± 0.3
FS bkg	11.3 ± 2.2	6.9 ± 1.5	2.4 ± 1.1	0.4 ± 0.3
WZ bkg	2.1 ± 1.5	1.6 ± 1.1	1.0 ± 0.7	0.5 ± 0.5
ZZ bkg	1.0 ± 0.5	1.1 ± 0.6	0.8 ± 0.4	0.7 ± 0.7
rare SM bkg	0.2 ± 0.1	0.3 ± 0.1	0.2 ± 0.1	0.2 ± 0.2
total bkg	21.7 ± 3.5	13.0 ± 2.2	6.1 ± 1.5	2.5 ± 0.9
data	?	?	?	?
significance	?	?	?	?

8 Interpretation

The results of this search will be interpreted in the context of simplified model spectra (SMS). For the inclusive analysis, we will use the T5zz model depicted in Fig. 1 (left). For the targeted analysis, we will use the $WZ + E_T^{\text{miss}}$ model depicted in Fig. 1 (right), and a GMSB model which produces a signature of $ZZ + E_T^{\text{miss}}$. For the $WZ + E_T^{\text{miss}}$ model (GMSB $ZZ + E_T^{\text{miss}}$ model), the results of this analysis will be combined with the results of searches for charginos and neutralinos in the trilepton (quadlepton) final state.

9 Summary

This note presents a search for BSM physics in final states with leptonically-decaying Z bosons, jets, and E_T^{miss} . Two strategies were pursued. The first is an inclusive approach which targets BSM scenarios with Z bosons produced in the decays of strongly-interacting particles. The second is a targeted approach which focuses on BSM scenarios where the Z bosons are produced in the decays of weakly-interacting particles. The main backgrounds are estimated with data-driven techniques. Good agreement is observed between the data and the predicted backgrounds in the control regions defined by $E_T^{\text{miss}} < 100$ GeV. The data yields in the signal region of the inclusive analysis will be presented when the decision to unblind the Z region of the edge analysis is taken. The data yields of the targeted analysis will be presented after completion of signal optimization studies.

References

- [1] CMS Collaboration, “Search for physics beyond the standard model in events with a Z boson, jets, and missing transverse energy in pp collisions at $\sqrt{s} = 7$ TeV,” arXiv:1204.3774v1 [hep-ex].
- [2] SUS-12-006, paper draft
- [3] <https://twiki.cern.ch/twiki/bin/viewauth/CMS/EgammaCutBasedIdentification>
- [4] <https://twiki.cern.ch/twiki/bin/viewauth/CMS/EgammaEARhoCorrection>
- [5] <https://twiki.cern.ch/twiki/bin/view/CMSPublic/SWGuideMuonId>
- [6] M. Chen, AN 2012/237 “Interpretation of the Same-Sign di-leptons with bjets and MET search”

A Results for the “edge analysis” SUS-12-019

The Aachen and ETH groups have reported an excess of low-mass, opposite-sign same-flavor events (see AN 2012/200 and AN 2012/231). In App. A.1 we derive predictions for the Z background in the Z mass regions for the two signal regions used for this analysis, and use these predictions to derive an estimate of the low-mass γ^*/Z contributions using an extrapolation technique commonly referred to as the “ $R_{out/in}$ ” technique.

A.1 Z Background Predictions for the “Edge Analysis”

The two signal regions of the edge analysis are defined as:

- Low- E_T^{miss} signal region (ETH)
 - 2 $p_T > 20$ GeV leptons with $|\eta| < 2.4$
 - At least 3 jets ($p_T > 40$ GeV, $|\eta| < 3$)
 - $E_T^{\text{miss}} > 100$ GeV
- High- E_T^{miss} signal region (Aachen)
 - leading lepton $p_T > 20$ GeV, trailing lepton $p_T > 10$ GeV, both with $|\eta| < 2.4$
 - At least 2 jets ($p_T > 40$ GeV, $|\eta| < 3$) with scalar sum $H_T > 100$ GeV
 - $E_T^{\text{miss}} > 150$ GeV

We begin with a synchronization exercise to make sure that we can reproduce the ETH/Aachen results. In Table 12 we display the yields in the Z mass regions of the 2 signal regions and compare these to results from the ETH group. In general we are synchronized to 3% or better in all channels. Note that for the purposes of this exercise we include an additional dimuon trigger (HLT_Mu17_TkMu8) which is not yet included in the results that follow. The inclusion of this trigger adds 3 $\mu\mu$ events in both the low E_T^{miss} and high E_T^{miss} signal regions.

Table 12: Summary of the synchronization exercise with the ETH group with 9.2 fb^{-1} . The yields in the Z mass region ($81 < m_{\ell\ell} < 101$ GeV) are displayed for the low E_T^{miss} and high E_T^{miss} signal regions.

low E_T^{miss} signal region	UCSB-UCSD-FNAL	ETH
ee	125	123
$\mu\mu$	166	164
$e\mu$	186	186
high E_T^{miss} signal region	UCSB-UCSD-FNAL	ETH
ee	75	72
$\mu\mu$	95	94
$e\mu$	113	113

In order to adapt the E_T^{miss} templates method to predict the Z background in these regions, we make minor modifications to the flavor-symmetric (FS) scaling factor K and to the binning used for the E_T^{miss} templates. The FS background is estimated using $e\mu$ events in data. To improve the precision of this background estimate, the dilepton mass requirement is not applied, and we apply a scaling factor K , which is the efficiency for $e\mu$ events to fall in the Z mass window, extracted from MC. The values of K for various E_T^{miss} intervals for the high- E_T^{miss} region (using $p_T > (20,10)$ GeV leptons and at least 2 jets) are shown in Fig. 12. Based on this plot we choose $K = 0.13 \pm 0.02$ for E_T^{miss} signal regions up to 200 GeV; for E_T^{miss} 200-300 GeV and $E_T^{\text{miss}} > 300$ GeV we inflate the uncertainty to $K = 0.13 \pm 0.04$ and $K = 0.13 \pm 0.05$, respectively, due to the limited statistical precision. The values of K for the low- E_T^{miss} region (using $p_T > (20,20)$ GeV leptons and at least 3 jets) are shown in Fig. 13. Based on this plot we choose $K = 0.14 \pm 0.02$ for E_T^{miss} signal regions up to 200 GeV; for E_T^{miss} 200-300 GeV and $E_T^{\text{miss}} > 300$ GeV we inflate the uncertainty to $K = 0.14 \pm 0.03$ and $K = 0.14 \pm 0.07$, respectively. In addition, we change the jet p_T threshold for the E_T^{miss} templates jet multiplicity binning from 30 to 40 GeV, and change the H_T bins to (0,80,100,150,200,250,300,5000) GeV.

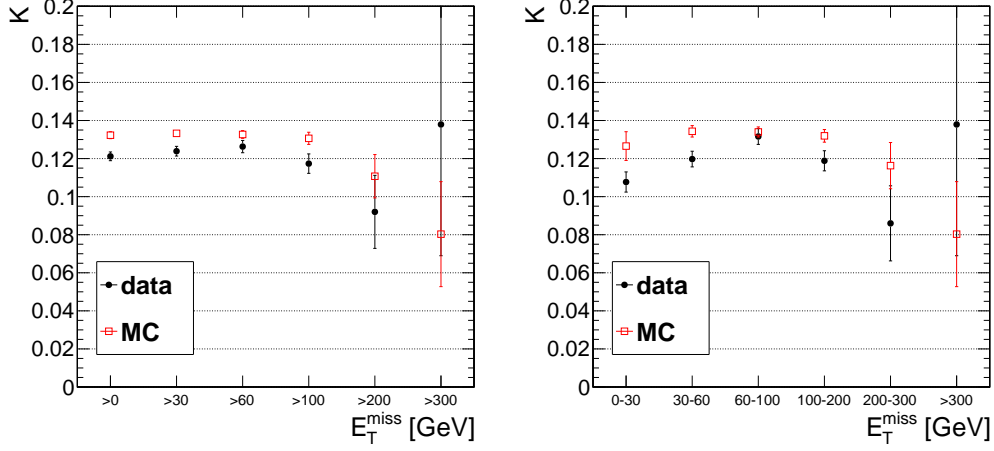


Figure 12: The efficiency for $e\mu$ events to satisfy the dilepton mass requirement, K , in data and simulation for inclusive E_T^{miss} intervals (left) and exclusive E_T^{miss} intervals (right) for the dilepton $p_T > (20,10)$ GeV selection with at least 2 $p_T > 40$ GeV jets (used for the high E_T^{miss} signal region).

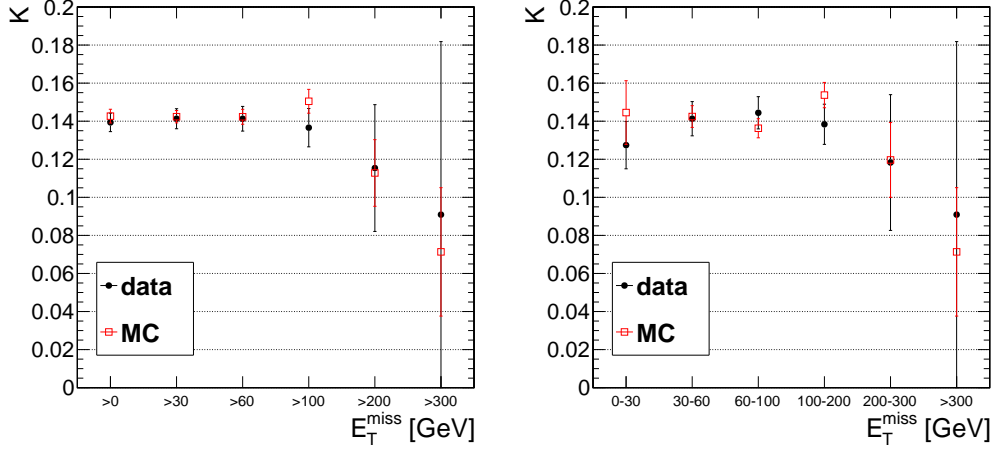


Figure 13: The efficiency for $e\mu$ events to satisfy the dilepton mass requirement, K , in data and simulation for inclusive E_T^{miss} intervals (left) and exclusive E_T^{miss} intervals (right) for the dilepton $p_T > (20,20)$ GeV selection with at least 3 $p_T > 40$ GeV jets (used for the low E_T^{miss} signal region).

The strategy is to select $Z \rightarrow \ell\ell$ candidates ($81 < m_{\ell\ell} < 101$ GeV) with jet requirements corresponding to the low- E_T^{miss} and high- E_T^{miss} signal regions, and compare the observed E_T^{miss} distribution to the sum of the predictions from the $Z + \text{jets}$ background (from the E_T^{miss} templates method based on the $\gamma + \text{jets}$ data control sample), the flavor-symmetric background predicted from $e\mu$ data events, and MC contributions from WZ/ZZ , as well as the rare SM processes with Z bosons ($t\bar{t}Z$ and ZZZ , ZZW , ZWW).

The results of the low E_T^{miss} signal region are displayed in Fig. 14 and summarized in Table 13, separately for the Run2012A+B data (5.1 fb^{-1}) and Run2012C data (4.1 fb^{-1}). In the Run2012A+B data, we observed a 1.6σ excess for $E_T^{\text{miss}} > 100$ GeV, corresponding to the low E_T^{miss} signal region. However, this excess does not persist in Run2012C data, where we observe good agreement between the data and the predicted background. In the combined Run2012A+B+C data (Fig. 16 and Table 15) we observe reasonable agreement over the full E_T^{miss} range. In the $E_T^{\text{miss}} > 100$ GeV region we observe 288 events with a predicted background of 251 ± 33 , representing an excess of 1.0σ .

The results of the high E_T^{miss} signal region are displayed in Fig. 15 and summarized in Table 14, separately for the Run2012A+B data (5.1 fb^{-1}) and Run2012C data (4.1 fb^{-1}). In both periods we observe good agreement between the data and predicted background over the full E_T^{miss} range. In the $E_T^{\text{miss}} > 150$ GeV region corresponding to the high E_T^{miss} signal region in the full sample, we observe 167 events with a predicted background of 177 ± 25 events, representing a deficit of -0.4σ .

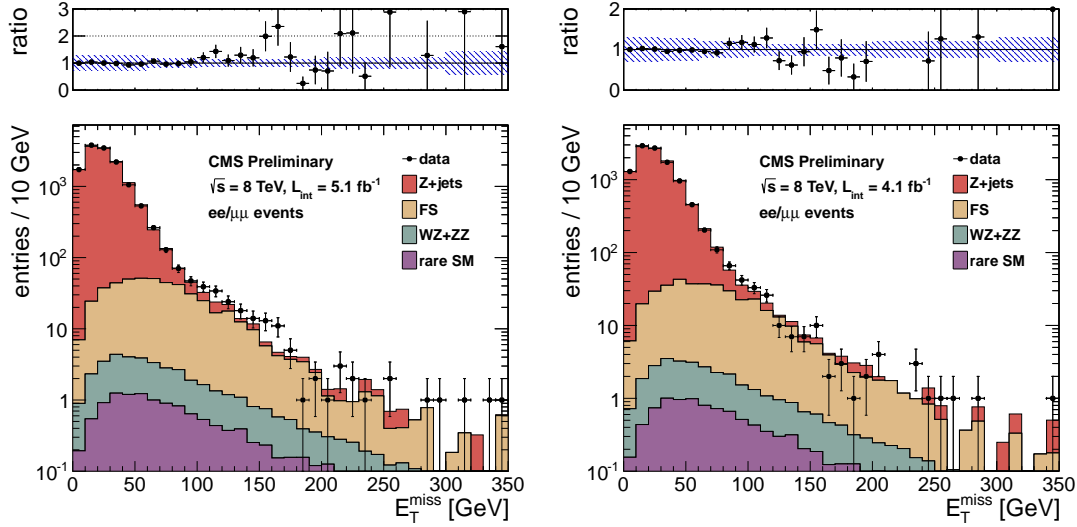


Figure 14: Results for the low E_T^{miss} signal region. The results for 5.1 fb^{-1} 2012A+B data are displayed on the left, the results for 4.1 fb^{-1} 2012C data are displayed on the right. The observed E_T^{miss} distribution (black points) is compared with the sum of the predicted E_T^{miss} distributions from Z+jets, flavor-symmetric backgrounds, WZ+ZZ backgrounds, and rare SM backgrounds. The ratio of observed to predicted yields in each bin is indicated. The error bars indicate the statistical uncertainty in the data and the shaded band indicates the total background uncertainty.

Table 13: Results for the low E_T^{miss} signal region. The results for 5.1 fb^{-1} 2012A+B data are displayed in the top table, the results for 4.1 fb^{-1} 2012C data are displayed in the bottom table. The total background is the sum of the Z + jets background predicted from the E_T^{miss} templates method (Z + jets bkg), the flavor-symmetric background predicted from $e\mu$ events (FS bkg), the WZ and ZZ backgrounds predicted from MC (WZ bkg and ZZ bkg) and the rare SM backgrounds. All uncertainties include both the statistical and systematic components. The Gaussian significance of the deviation between the data and total background is indicated for signal regions with at least 20 observed events.

	$E_T^{\text{miss}} > 0 \text{ GeV}$	$E_T^{\text{miss}} > 30 \text{ GeV}$	$E_T^{\text{miss}} > 60 \text{ GeV}$	$E_T^{\text{miss}} > 100 \text{ GeV}$	$E_T^{\text{miss}} > 200 \text{ GeV}$	$E_T^{\text{miss}} > 300 \text{ GeV}$
Z + jets bkg	12870 ± 3862	4118 ± 1236	356 ± 107	27.5 ± 8.5	2.6 ± 1.1	0.3 ± 0.3
FS bkg	451 ± 70	389 ± 61	256 ± 40	99.1 ± 15.8	6.9 ± 1.8	1.0 ± 0.6
WZ bkg	24.1 ± 16.9	19.5 ± 13.7	11.8 ± 8.3	5.6 ± 3.9	1.1 ± 1.0	0.2 ± 0.2
ZZ bkg	4.3 ± 2.2	3.9 ± 2.0	3.0 ± 1.5	1.9 ± 1.0	0.5 ± 0.4	0.1 ± 0.1
rare SM bkg	12.2 ± 6.1	10.5 ± 5.3	6.9 ± 3.5	3.5 ± 1.8	0.7 ± 0.6	0.2 ± 0.2
total bkg	13362 ± 3862	4541 ± 1238	634 ± 115	138 ± 18	11.8 ± 2.5	1.8 ± 0.8
data	13412	4461	684	175	14	3
significance	0.0σ	-0.1σ	0.4σ	1.6σ	0.5σ	
	$E_T^{\text{miss}} > 0 \text{ GeV}$	$E_T^{\text{miss}} > 30 \text{ GeV}$	$E_T^{\text{miss}} > 60 \text{ GeV}$	$E_T^{\text{miss}} > 100 \text{ GeV}$	$E_T^{\text{miss}} > 200 \text{ GeV}$	$E_T^{\text{miss}} > 300 \text{ GeV}$
Z + jets bkg	10203 ± 3061	3449 ± 1035	320 ± 97	20.5 ± 6.3	2.1 ± 0.6	0.8 ± 0.2
FS bkg	356 ± 56	307 ± 48	201 ± 32	84.5 ± 13.5	7.2 ± 1.9	0.6 ± 0.4
WZ bkg	19.4 ± 13.6	15.7 ± 11.0	9.5 ± 6.6	4.5 ± 3.2	0.9 ± 0.8	0.2 ± 0.2
ZZ bkg	3.5 ± 1.8	3.1 ± 1.6	2.4 ± 1.2	1.5 ± 0.8	0.4 ± 0.4	0.1 ± 0.1
rare SM bkg	9.8 ± 4.9	8.5 ± 4.3	5.5 ± 2.8	2.8 ± 1.5	0.6 ± 0.5	0.1 ± 0.1
total bkg	10592 ± 3062	3783 ± 1036	538 ± 102	114 ± 15	11.2 ± 2.2	1.8 ± 0.5
data	10587	3673	533	113	12	1
significance	-0.0σ	-0.1σ	-0.0σ	-0.0σ		

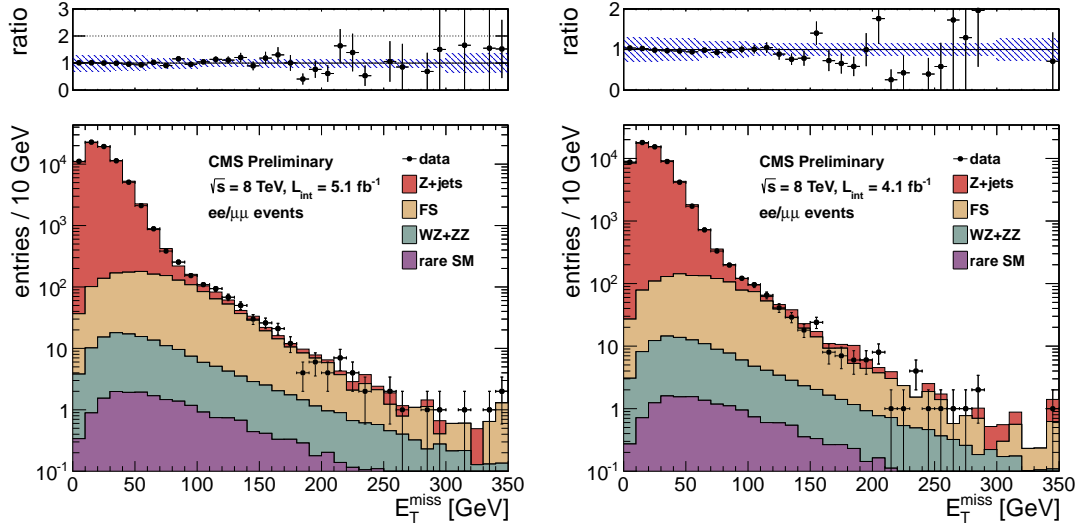


Figure 15: Results of for the high E_T^{miss} signal region. The results for 5.1 fb^{-1} 2012A+B data are displayed on the left, the results for 4.1 fb^{-1} 2012C data are displayed on the right. The observed E_T^{miss} distribution (black points) is compared with the sum of the predicted E_T^{miss} distributions from Z + jets , flavor-symmetric backgrounds, WZ+ZZ backgrounds, and rare SM backgrounds. The ratio of observed to predicted yields in each bin is indicated. The error bars indicate the statistical uncertainty in the data and the shaded band indicates the total background uncertainty.

Table 14: Results for the high E_T^{miss} signal region. The results for 5.1 fb^{-1} 2012A+B data are displayed in the top table, the results for 4.1 fb^{-1} 2012C data are displayed in the bottom table. The total background is the sum of the Z + jets background predicted from the E_T^{miss} templates method (Z + jets bkg), the flavor-symmetric background predicted from $e\mu$ events (FS bkg), the WZ and ZZ backgrounds predicted from MC (WZ bkg and ZZ bkg) and the rare SM backgrounds. All uncertainties include both the statistical and systematic components. The Gaussian significance of the deviation between the data and total background is indicated for signal regions with at least 20 observed events.

	$E_T^{\text{miss}} > 0 \text{ GeV}$	$E_T^{\text{miss}} > 30 \text{ GeV}$	$E_T^{\text{miss}} > 60 \text{ GeV}$	$E_T^{\text{miss}} > 100 \text{ GeV}$	$E_T^{\text{miss}} > 150 \text{ GeV}$	$E_T^{\text{miss}} > 300 \text{ GeV}$
Z + jets bkg	71975 ± 21593	19573 ± 5873	1182 ± 355	70.7 ± 21.4	13.6 ± 4.2	0.4 ± 0.4
FS bkg	1540 ± 255	1293 ± 214	823 ± 136	313 ± 52	68.6 ± 11.7	2.4 ± 1.1
WZ bkg	115.9 ± 81.2	91.8 ± 64.3	52.1 ± 36.5	22.4 ± 15.7	8.9 ± 6.3	0.8 ± 0.8
ZZ bkg	22.6 ± 11.3	20.3 ± 10.2	15.1 ± 7.6	8.8 ± 4.5	4.3 ± 2.3	0.5 ± 0.5
rare SM bkg	20.6 ± 10.3	17.9 ± 9.0	12.0 ± 6.1	6.3 ± 3.2	2.8 ± 1.5	0.3 ± 0.3
total bkg	73674 ± 21595	20996 ± 5877	2084 ± 382	421 ± 59	98.1 ± 14.2	4.5 ± 1.5
data	73711	20601	2121	446	95	4
significance	0.0σ	-0.1σ	0.1σ	0.4σ	-0.2σ	
	$E_T^{\text{miss}} > 0 \text{ GeV}$	$E_T^{\text{miss}} > 30 \text{ GeV}$	$E_T^{\text{miss}} > 60 \text{ GeV}$	$E_T^{\text{miss}} > 100 \text{ GeV}$	$E_T^{\text{miss}} > 150 \text{ GeV}$	$E_T^{\text{miss}} > 300 \text{ GeV}$
Z + jets bkg	57206 ± 17163	15965 ± 4790	1040 ± 313	68.3 ± 21.5	17.5 ± 6.0	1.4 ± 0.4
FS bkg	1206 ± 200	1015 ± 168	649 ± 108	244 ± 41	48.1 ± 8.3	1.3 ± 0.6
WZ bkg	93.2 ± 65.3	73.8 ± 51.7	41.9 ± 29.4	18.0 ± 12.7	7.1 ± 5.1	0.7 ± 0.7
ZZ bkg	18.2 ± 9.1	16.3 ± 8.2	12.1 ± 6.1	7.1 ± 3.6	3.4 ± 1.8	0.4 ± 0.4
rare SM bkg	16.6 ± 8.3	14.4 ± 7.2	9.7 ± 4.9	5.1 ± 2.6	2.3 ± 1.2	0.3 ± 0.3
total bkg	58541 ± 17164	17084 ± 4793	1753 ± 332	343 ± 48	78.4 ± 11.7	4.0 ± 1.1
data	58478	16494	1690	321	72	1
significance	-0.0σ	-0.1σ	-0.2σ	-0.4σ	-0.4σ	

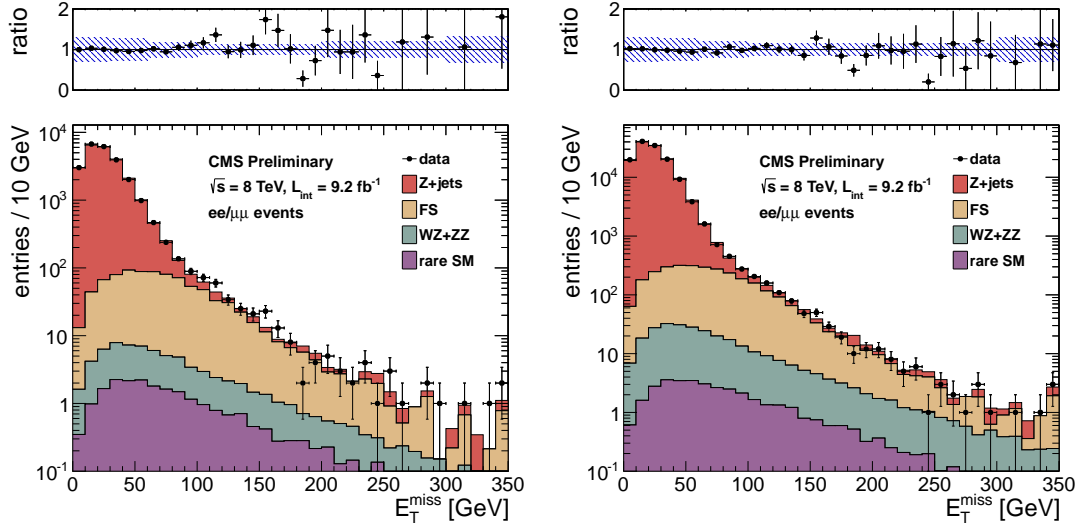


Figure 16: Results of for the low E_T^{miss} (left) and high E_T^{miss} (right) signal regions for the full 9.2 fb^{-1} sample. The observed E_T^{miss} distribution (black points) is compared with the sum of the predicted E_T^{miss} distributions from $Z + \text{jets}$, flavor-symmetric backgrounds, $WZ+ZZ$ backgrounds, and rare SM backgrounds. The ratio of observed to predicted yields in each bin is indicated. The error bars indicate the statistical uncertainty in the data and the shaded band indicates the total background uncertainty.

Table 15: Results for the low E_T^{miss} signal region (top table) and high E_T^{miss} signal region (bottom table). The total background is the sum of the $Z + \text{jets}$ background predicted from the E_T^{miss} templates method ($Z + \text{jets}$ bkg), the flavor-symmetric background predicted from $e\mu$ events (FS bkg), the WZ and ZZ backgrounds predicted from MC (WZ bkg and ZZ bkg) and the rare SM backgrounds. All uncertainties include both the statistical and systematic components. The Gaussian significance of the deviation between the data and total background is indicated for signal regions with at least 20 observed events.

	$E_T^{\text{miss}} > 0 \text{ GeV}$	$E_T^{\text{miss}} > 30 \text{ GeV}$	$E_T^{\text{miss}} > 60 \text{ GeV}$	$E_T^{\text{miss}} > 100 \text{ GeV}$	$E_T^{\text{miss}} > 200 \text{ GeV}$	$E_T^{\text{miss}} > 300 \text{ GeV}$
$Z + \text{jets}$ bkg	23072 ± 6922	7566 ± 2270	674 ± 203	47.9 ± 14.6	4.7 ± 1.6	1.1 ± 0.4
FS bkg	807 ± 126	695 ± 108	457 ± 71	184 ± 29	14.1 ± 3.4	1.5 ± 0.9
WZ bkg	43.5 ± 30.5	35.1 ± 24.6	21.3 ± 14.9	10.0 ± 7.1	1.9 ± 1.7	0.4 ± 0.4
ZZ bkg	7.8 ± 3.9	7.0 ± 3.6	5.4 ± 2.8	3.3 ± 1.8	0.9 ± 0.8	0.2 ± 0.2
rare SM bkg	22.0 ± 11.0	19.0 ± 9.6	12.4 ± 6.3	6.3 ± 3.3	1.3 ± 1.1	0.3 ± 0.3
total bkg	23952 ± 6923	8323 ± 2273	1170 ± 216	251 ± 33	22.8 ± 4.4	3.5 ± 1.1
data	23999	8134	1217	288	26	4
significance	0.0σ	-0.1σ	0.2σ	1.0σ	0.5σ	
	$E_T^{\text{miss}} > 0 \text{ GeV}$	$E_T^{\text{miss}} > 30 \text{ GeV}$	$E_T^{\text{miss}} > 60 \text{ GeV}$	$E_T^{\text{miss}} > 100 \text{ GeV}$	$E_T^{\text{miss}} > 150 \text{ GeV}$	$E_T^{\text{miss}} > 300 \text{ GeV}$
$Z + \text{jets}$ bkg	129184 ± 38756	35565 ± 10670	2225 ± 668	140 ± 43	31.6 ± 10.1	1.7 ± 0.6
FS bkg	2746 ± 454	2308 ± 382	1471 ± 243	557 ± 92	117 ± 20	3.7 ± 1.6
WZ bkg	209.2 ± 146.4	165.6 ± 115.9	94.1 ± 65.9	40.5 ± 28.4	16.0 ± 11.3	1.5 ± 1.5
ZZ bkg	40.8 ± 20.4	36.6 ± 18.4	27.2 ± 13.7	16.0 ± 8.1	7.7 ± 4.1	0.9 ± 0.9
rare SM bkg	37.2 ± 18.7	32.2 ± 16.2	21.7 ± 10.9	11.4 ± 5.8	5.1 ± 2.8	0.6 ± 0.6
total bkg	132217 ± 38759	38108 ± 10678	3839 ± 714	765 ± 106	177 ± 25	8.4 ± 2.5
data	132189	37095	3811	767	167	5
significance	-0.0σ	-0.1σ	-0.0σ	0.0σ	-0.4σ	

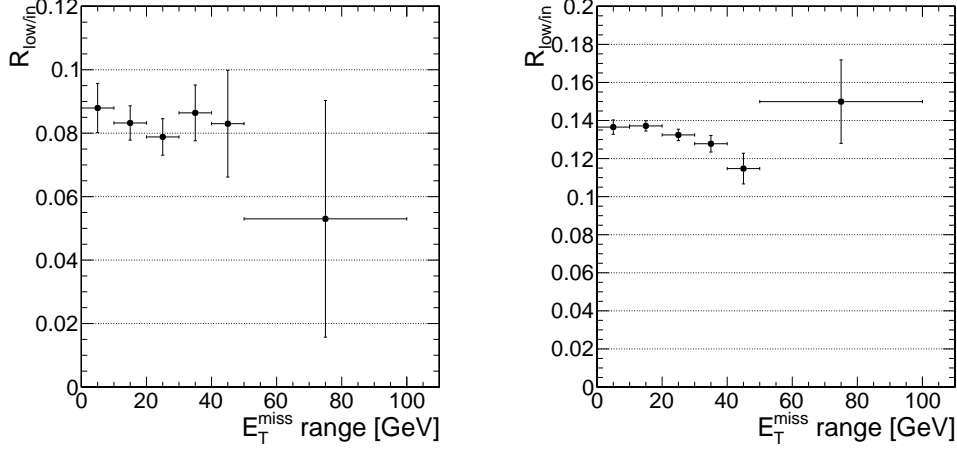


Figure 17: The ratio $R_{low/in}$ of low mass ($15 < m_{\ell\ell} < 70$ GeV) to on-Z ($81 < m_{\ell\ell} < 101$ GeV) events, as a function of the E_T^{miss} requirement. The left plot corresponds to the low E_T^{miss} signal region ($2 p_T > 20$ GeV leptons with at least 3 jets), the right plot corresponds to the high E_T^{miss} signal region ($p_T > (20,10)$ GeV leptons with at least 2 jets).

Given a prediction for the Z background in the Z mass window, we can extrapolate to estimate the low mass γ^*/Z contribution. We extract the ratio $R_{low/in}$ of low-mass to on-shell Z events from data, correcting for the contribution from flavor-symmetric backgrounds, according to:

$$R_{low/in} = (N_{SF}^{low} - N_{OF}^{low}) / (N_{SF}^{in} - N_{OF}^{in}). \quad (2)$$

Here SF and OF refer to the same-flavor and opposite-flavor data yields in the “low” ($15 < m_{\ell\ell} < 70$ GeV) and “in” ($81 < m_{\ell\ell} < 101$ GeV) dilepton mass regions. To predict the low-mass γ^*/Z contribution, we scale the total predicted Z background by this quantity, which is displayed in Fig. 17. Here we measure $R_{low/in}$ in several E_T^{miss} regions, and assess the uncertainty based on the variation with respect to E_T^{miss} . Based on this plot we choose $R_{low/in} = 0.08 \pm 0.02$ for the low E_T^{miss} signal region and $R_{low/in} = 0.13 \pm 0.03$ for the high E_T^{miss} region.

We find the following results for the first 5.1 fb^{-1} . For the low E_T^{miss} signal region, the total predicted Z background in the Z mass region is 39 ± 9.6 (sum of the Z + jets , WZ+ZZ, and rare SM backgrounds from Table 13, $E_T^{\text{miss}} > 100 \text{ GeV}$ region), resulting in a γ^*/Z prediction of 3.1 ± 1.1 events. For the high E_T^{miss} signal region, the total predicted Z background in the Z mass region is 30 ± 8.1 (sum of the Z + jets , WZ+ZZ, and rare SM backgrounds from Table 14, $E_T^{\text{miss}} > 150 \text{ GeV}$ region), resulting in a γ^*/Z prediction of 3.8 ± 1.4 events. Hence we summarize the 5.1 fb^{-1} results as:

- Low E_T^{miss} signal region

- Total predicted background in Z mass region: 138 ± 18 events
- Total observed yield in Z mass region: 175 events ($+1.6\sigma$)
- Low-mass γ^*/Z prediction: 3.1 ± 1.1 events

- High E_T^{miss} signal region

- Total predicted background in Z mass region: 98 ± 14 events
- Total observed yield in Z mass region: 95 events (-0.2σ)
- Low-mass γ^*/Z prediction: 3.8 ± 1.4 events

We find the following results for the full 9.2 fb^{-1} . For the low E_T^{miss} signal region, the total predicted Z background in the Z mass region is 68 ± 17 (sum of the Z + jets , WZ+ZZ, and rare SM backgrounds from Table 15, $E_T^{\text{miss}} > 100 \text{ GeV}$ region), resulting in a γ^*/Z prediction of 5.4 ± 1.9 events. For the high E_T^{miss} signal region, the total predicted Z background in the Z mass region is 60 ± 16 (sum of the Z + jets , WZ+ZZ, and rare SM backgrounds from Table 15, $E_T^{\text{miss}} > 150 \text{ GeV}$ region), resulting in a γ^*/Z prediction of 7.9 ± 2.7 events. Hence we summarize the 9.2 fb^{-1} results as:

- Low E_T^{miss} signal region

- Total predicted background in Z mass region: 251 ± 33 events
- Total observed yield in Z mass region: 288 events ($+1.0\sigma$)
- Low-mass γ^*/Z prediction: 5.4 ± 1.9 events

- High E_T^{miss} signal region

- Total predicted background in Z mass region: 177 ± 25 events
- Total observed yield in Z mass region: 167 events (-0.4σ)
- Low-mass γ^*/Z prediction: 7.9 ± 2.7 events

B Results in the ee and $\mu\mu$ Channels

In this section we provide the results of the inclusive and targeted searches, separately in the ee and $\mu\mu$ channels. The E_T^{miss} distributions in the inclusive analysis for the ee channel are displayed in Fig. 18 and the signal region yields are presented in Table 16. The E_T^{miss} distributions in the inclusive analysis for the $\mu\mu$ channel are displayed in Fig. 19 and the signal region yields are presented in Table 17.

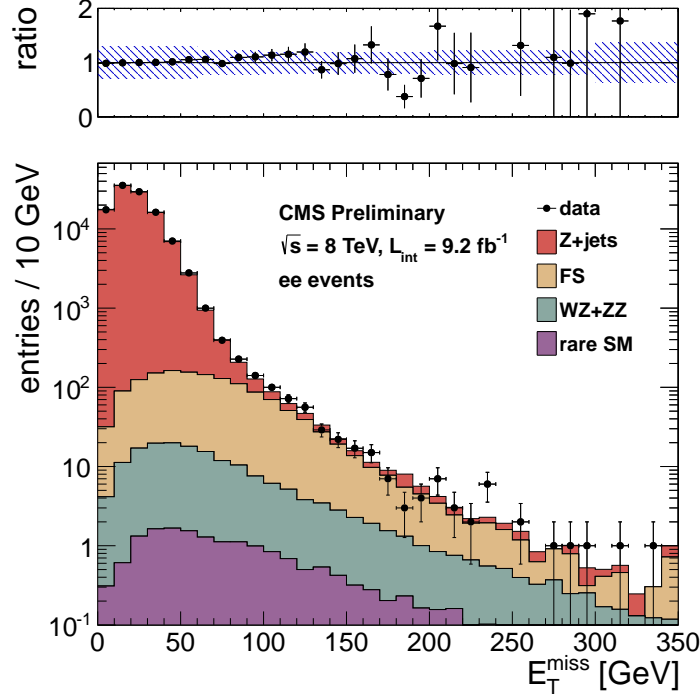


Figure 18: Results of the inclusive analysis in the ee channel. The observed E_T^{miss} distribution (black points) is compared with the sum of the predicted E_T^{miss} distributions from Z + jets , flavor-symmetric backgrounds, and WZ+ZZ backgrounds. The ratio of observed to predicted yields in each bin is indicated. The error bars indicate the statistical uncertainty in the data and the shaded band indicates the total background uncertainty.

Table 16: Summary of results in the inclusive analysis in the ee channel. The total background is the sum of the Z + jets background predicted from the E_T^{miss} templates method (Z + jets bkg), the flavor-symmetric background predicted from $e\mu$ events (FS bkg), and the WZ and ZZ backgrounds predicted from MC (WZ bkg and ZZ bkg). All uncertainties include both the statistical and systematic components. The Gaussian significance of the deviation between the data and total background is indicated for signal regions with at least 20 observed events.

	E_T^{miss} 0–30 GeV	E_T^{miss} 30–60 GeV	E_T^{miss} 60–100 GeV	E_T^{miss} 100–200 GeV	E_T^{miss} 200–300 GeV	E_T^{miss} > 300 GeV
Z + jets bkg	82295 ± 24694	25206 ± 7570	1204 ± 371	54.8 ± 40.1	3.3 ± 1.1	0.6 ± 0.2
FS bkg	214 ± 40	411 ± 77	426 ± 80	218 ± 41	10.2 ± 3.3	1.3 ± 0.8
WZ bkg	26.9 ± 18.9	45.7 ± 32.0	33.4 ± 23.4	18.3 ± 12.8	2.6 ± 1.8	0.8 ± 0.8
ZZ bkg	3.3 ± 1.6	6.9 ± 3.5	7.4 ± 3.7	7.0 ± 3.5	1.5 ± 0.8	0.4 ± 0.4
rare SM bkg	2.2 ± 1.1	4.8 ± 2.4	4.5 ± 2.3	4.2 ± 2.1	0.8 ± 0.4	0.3 ± 0.3
total bkg	82542 ± 24694	25675 ± 7570	1675 ± 380	303 ± 59	18.5 ± 4.0	3.4 ± 1.3
data	82228	25989	1758	325	23	2
significance	-0.0σ	0.0σ	0.2σ	0.4σ	0.7σ	-0.7σ

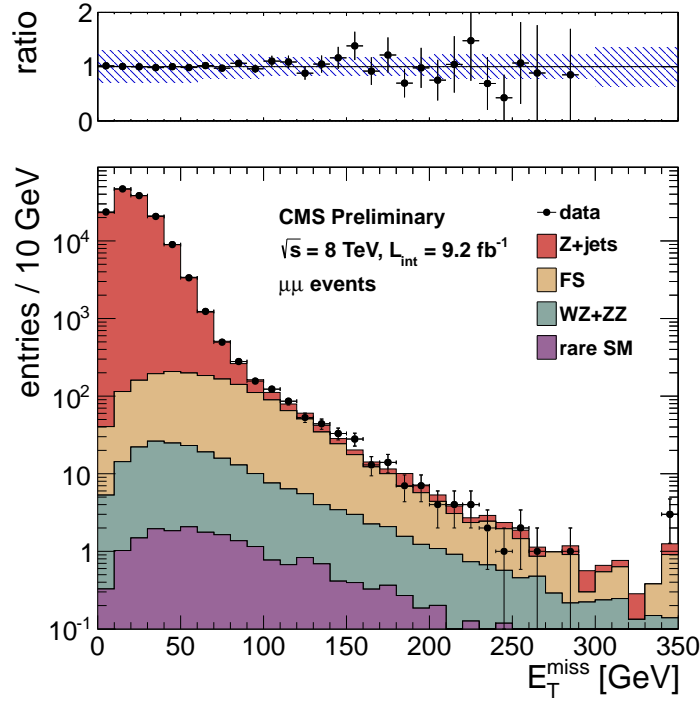


Figure 19: Results of the inclusive analysis in the $\mu\mu$ channel. The observed E_T^{miss} distribution (black points) is compared with the sum of the predicted E_T^{miss} distributions from Z + jets , flavor-symmetric backgrounds, and WZ+ZZ backgrounds. The ratio of observed to predicted yields in each bin is indicated. The error bars indicate the statistical uncertainty in the data and the shaded band indicates the total background uncertainty.

Table 17: Summary of results in the inclusive analysis in the $\mu\mu$ channel. The total background is the sum of the Z + jets background predicted from the E_T^{miss} templates method (Z + jets bkg), the flavor-symmetric background predicted from $e\mu$ events (FS bkg), and the WZ and ZZ backgrounds predicted from MC (WZ bkg and ZZ bkg). All uncertainties include both the statistical and systematic components. The Gaussian significance of the deviation between the data and total background is indicated for signal regions with at least 20 observed events.

	E_T^{miss} 0–30 GeV	E_T^{miss} 30–60 GeV	E_T^{miss} 60–100 GeV	E_T^{miss} 100–200 GeV	E_T^{miss} 200–300 GeV	E_T^{miss} > 300 GeV
Z + jets bkg	107821 ± 32348	32792 ± 9840	1541 ± 465	68.3 ± 27.7	4.1 ± 1.3	0.7 ± 0.3
FS bkg	274 ± 51	526 ± 98	545 ± 102	279 ± 52	13.1 ± 4.2	1.7 ± 1.1
WZ bkg	34.5 ± 24.2	59.1 ± 41.4	42.0 ± 29.4	22.9 ± 16.1	3.1 ± 2.2	0.8 ± 0.8
ZZ bkg	4.3 ± 2.2	9.2 ± 4.6	10.0 ± 5.0	9.2 ± 4.6	1.7 ± 0.9	0.6 ± 0.6
rare SM bkg	2.8 ± 1.4	5.9 ± 2.9	5.9 ± 3.0	4.9 ± 2.5	0.8 ± 0.4	0.3 ± 0.3
total bkg	108136 ± 32348	33393 ± 9840	2144 ± 477	385 ± 62	22.9 ± 5.0	4.1 ± 1.5
data	108565	32964	2163	408	19	3
significance	0.0σ	-0.0σ	0.0σ	0.4σ	-0.6σ	-0.5σ

390 The E_T^{miss} distributions in the targeted analysis for the ee channel are displayed in Fig. 20 and the signal region
 391 yields are presented in Table 18. The E_T^{miss} distributions in the inclusive analysis for the $\mu\mu$ channel are displayed
 392 in Fig. 21 and the signal region yields are presented in Table 19.

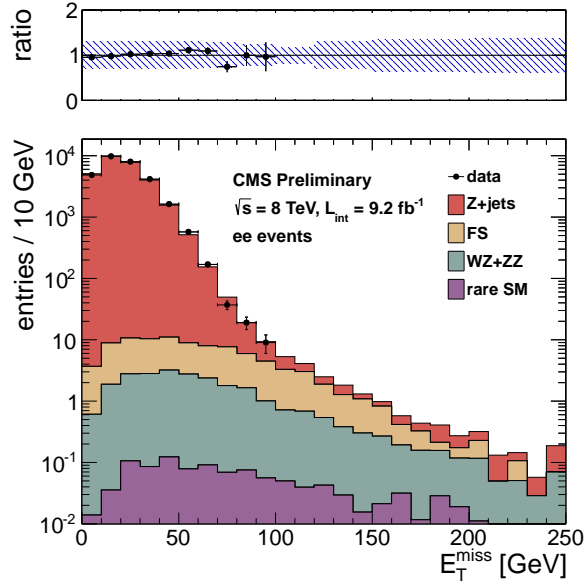


Figure 20: Results of the targeted analysis in the ee channel. The observed E_T^{miss} distribution (black points) is compared with the sum of the predicted E_T^{miss} distributions from Z + jets , flavor-symmetric backgrounds, and WZ+ZZ backgrounds. The ratio of observed to predicted yields in each bin is indicated. The error bars indicate the statistical uncertainty in the data and the shaded band indicates the total background uncertainty.

Table 18: Summary of results in the targeted analysis in the ee channel. The total background is the sum of the Z + jets background predicted from the E_T^{miss} templates method (Z + jets bkg), the flavor-symmetric background predicted from $e\mu$ events (FS bkg), and the WZ and ZZ backgrounds predicted from MC (WZ bkg and ZZ bkg). All uncertainties include both the statistical and systematic components. The Gaussian significance of the deviation between the data and total background is indicated for signal regions with at least 20 observed events.

	E_T^{miss} 0–30 GeV	E_T^{miss} 30–60 GeV	E_T^{miss} 60–80 GeV	E_T^{miss} 80–100 GeV
Z + jets bkg	22806 ± 6842	6065 ± 1820	188 ± 57	17.9 ± 6.2
FS bkg	17.9 ± 3.6	21.5 ± 4.3	11.5 ± 2.4	7.8 ± 1.7
WZ bkg	4.2 ± 2.9	6.8 ± 4.7	3.0 ± 2.1	1.8 ± 1.2
ZZ bkg	1.0 ± 0.5	1.7 ± 0.9	1.0 ± 0.5	0.8 ± 0.4
rare SM bkg	0.2 ± 0.1	0.3 ± 0.1	0.2 ± 0.1	0.1 ± 0.1
total bkg	22830 ± 6842	6095 ± 1820	204 ± 58	28.4 ± 6.5
data	22581	6344	206	28
significance	-0.0σ	0.1σ	0.0σ	-0.0σ
	E_T^{miss} 100–120 GeV	E_T^{miss} 120–150 GeV	E_T^{miss} 150–200 GeV	E_T^{miss} > 200 GeV
Z + jets bkg	3.1 ± 1.1	1.4 ± 1.4	0.7 ± 0.7	0.4 ± 0.1
FS bkg	4.9 ± 1.1	3.0 ± 0.7	1.1 ± 0.5	0.2 ± 0.1
WZ bkg	0.9 ± 0.6	0.7 ± 0.5	0.4 ± 0.3	0.2 ± 0.2
ZZ bkg	0.4 ± 0.2	0.4 ± 0.2	0.4 ± 0.2	0.3 ± 0.3
rare SM bkg	0.1 ± 0.0	0.1 ± 0.0	0.1 ± 0.1	0.1 ± 0.1
total bkg	9.4 ± 1.7	5.6 ± 1.7	2.7 ± 0.9	1.1 ± 0.4
data	?	?	?	?
significance	?	?	?	?

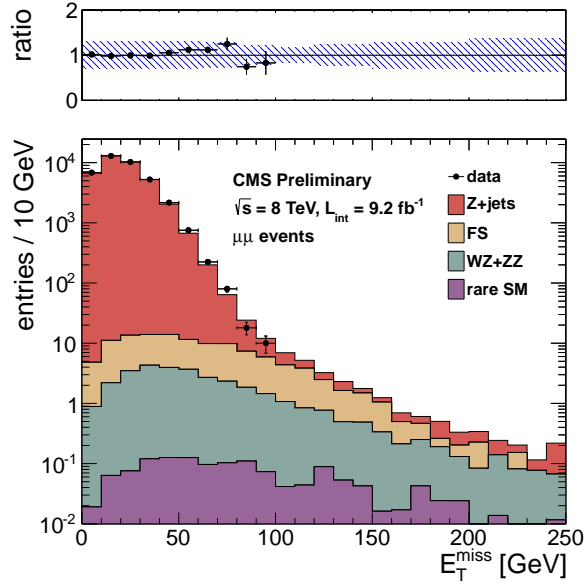


Figure 21: Results of the targeted analysis in the $\mu\mu$ channel. The observed E_T^{miss} distribution (black points) is compared with the sum of the predicted E_T^{miss} distributions from Z + jets , flavor-symmetric backgrounds, and WZ+ZZ backgrounds. The ratio of observed to predicted yields in each bin is indicated. The error bars indicate the statistical uncertainty in the data and the shaded band indicates the total background uncertainty.

Table 19: Summary of results in the targeted analysis in the $\mu\mu$ channel. The total background is the sum of the Z + jets background predicted from the E_T^{miss} templates method (Z + jets bkg), the flavor-symmetric background predicted from $e\mu$ events (FS bkg), and the WZ and ZZ backgrounds predicted from MC (WZ bkg and ZZ bkg). All uncertainties include both the statistical and systematic components. The Gaussian significance of the deviation between the data and total background is indicated for signal regions with at least 20 observed events.

	E_T^{miss} 0–30 GeV	E_T^{miss} 30–60 GeV	E_T^{miss} 60–80 GeV	E_T^{miss} 80–100 GeV
Z + jets bkg	30017 ± 9005	7950 ± 2385	245 ± 74	23.0 ± 7.2
FS bkg	23.0 ± 4.7	27.5 ± 5.6	14.7 ± 3.0	9.9 ± 2.1
WZ bkg	5.3 ± 3.7	9.2 ± 6.4	3.6 ± 2.5	2.1 ± 1.5
ZZ bkg	1.1 ± 0.6	2.4 ± 1.2	1.2 ± 0.6	1.0 ± 0.5
rare SM bkg	0.2 ± 0.1	0.4 ± 0.2	0.2 ± 0.1	0.2 ± 0.1
total bkg	30046 ± 9005	7990 ± 2385	264 ± 74	36.2 ± 7.6
data	29904	8132	304	28
significance	-0.0σ	0.1σ	0.5σ	-0.9σ
	E_T^{miss} 100–120 GeV	E_T^{miss} 120–150 GeV	E_T^{miss} 150–200 GeV	E_T^{miss} > 200 GeV
Z + jets bkg	3.9 ± 1.2	1.7 ± 1.2	0.9 ± 0.6	0.5 ± 0.1
FS bkg	6.3 ± 1.4	3.9 ± 0.9	1.4 ± 0.6	0.2 ± 0.2
WZ bkg	1.2 ± 0.9	0.9 ± 0.6	0.6 ± 0.4	0.3 ± 0.3
ZZ bkg	0.6 ± 0.3	0.7 ± 0.4	0.4 ± 0.2	0.4 ± 0.4
rare SM bkg	0.1 ± 0.0	0.2 ± 0.1	0.1 ± 0.1	0.1 ± 0.1
total bkg	12.1 ± 2.1	7.3 ± 1.7	3.4 ± 1.0	1.4 ± 0.5
data	?	?	?	?
significance	?	?	?	?

393 E_T^{miss} Templates from $\gamma + \text{jets}$ Sample

394 In this section we display the templates used for the inclusive analysis (red) and the targeted analysis (blue).

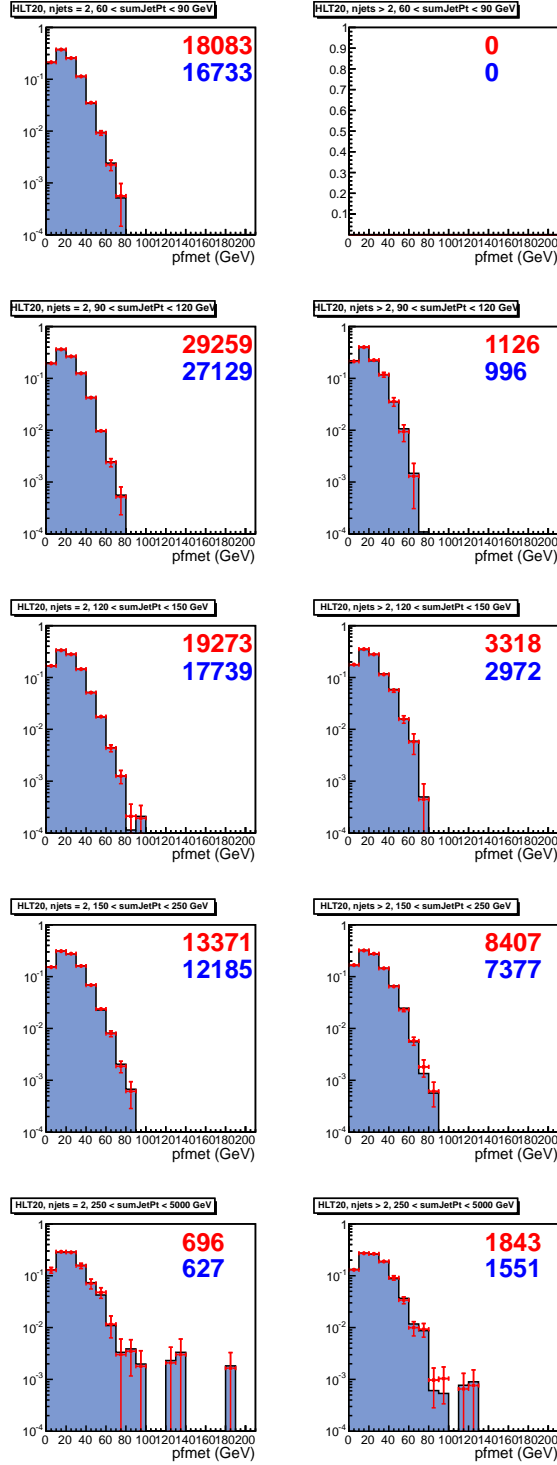


Figure 22: E_T^{miss} templates collected with the $p_T > 22$ GeV single photon trigger. The number in red (blue) indicates the number of entries in the template for the inclusive (targeted) analysis.

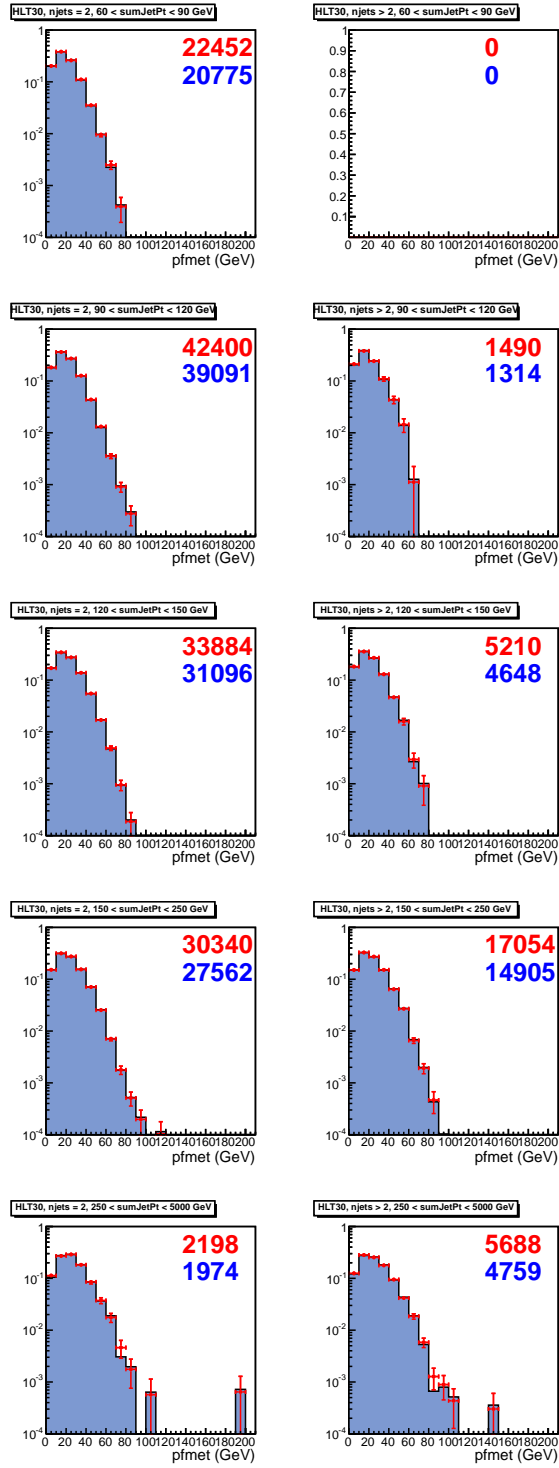


Figure 23: E_T^{miss} templates collected with the $p_T > 36$ GeV single photon trigger. The number in red (blue) indicates the number of entries in the template for the inclusive (targeted) analysis.

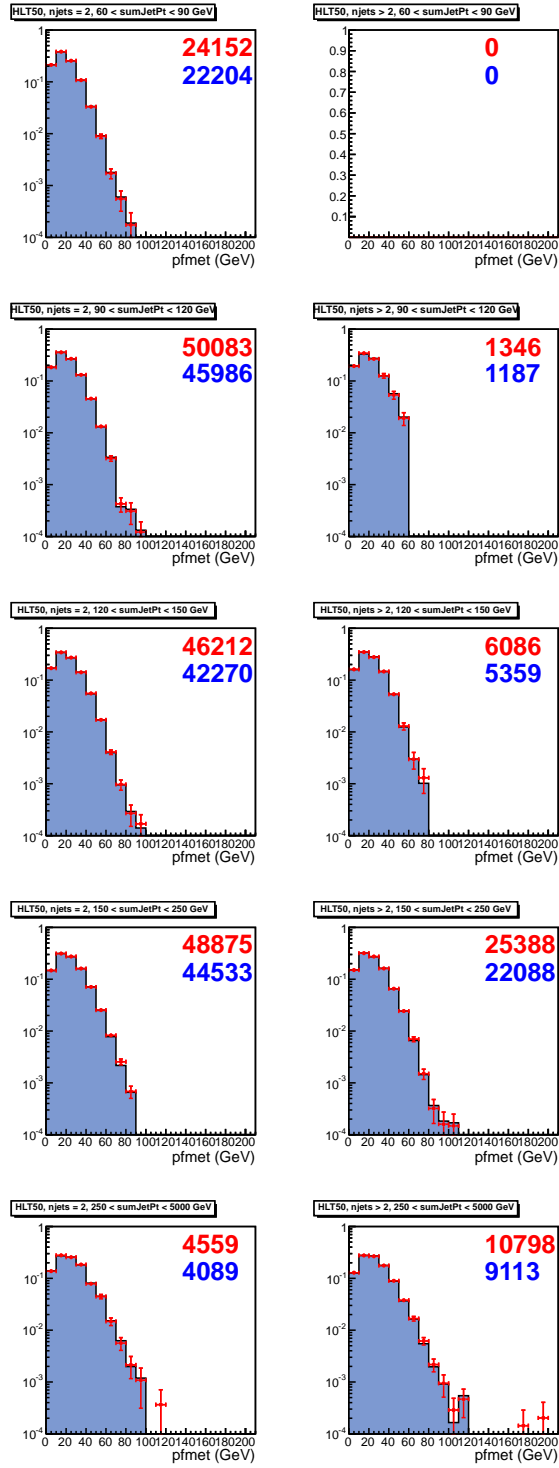


Figure 24: E_T^{miss} templates collected with the $p_T > 50$ GeV single photon trigger. The number in red (blue) indicates the number of entries in the template for the inclusive (targeted) analysis.

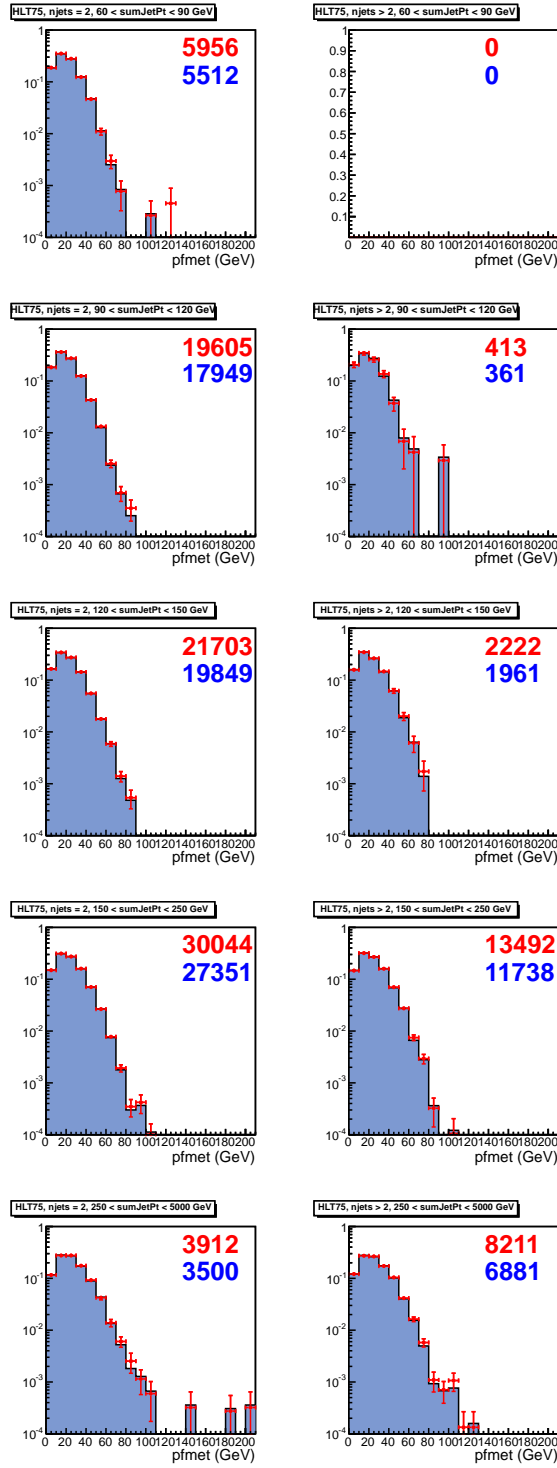


Figure 25: E_T^{miss} templates collected with the $p_T > 75$ GeV single photon trigger. The number in red (blue) indicates the number of entries in the template for the inclusive (targeted) analysis.

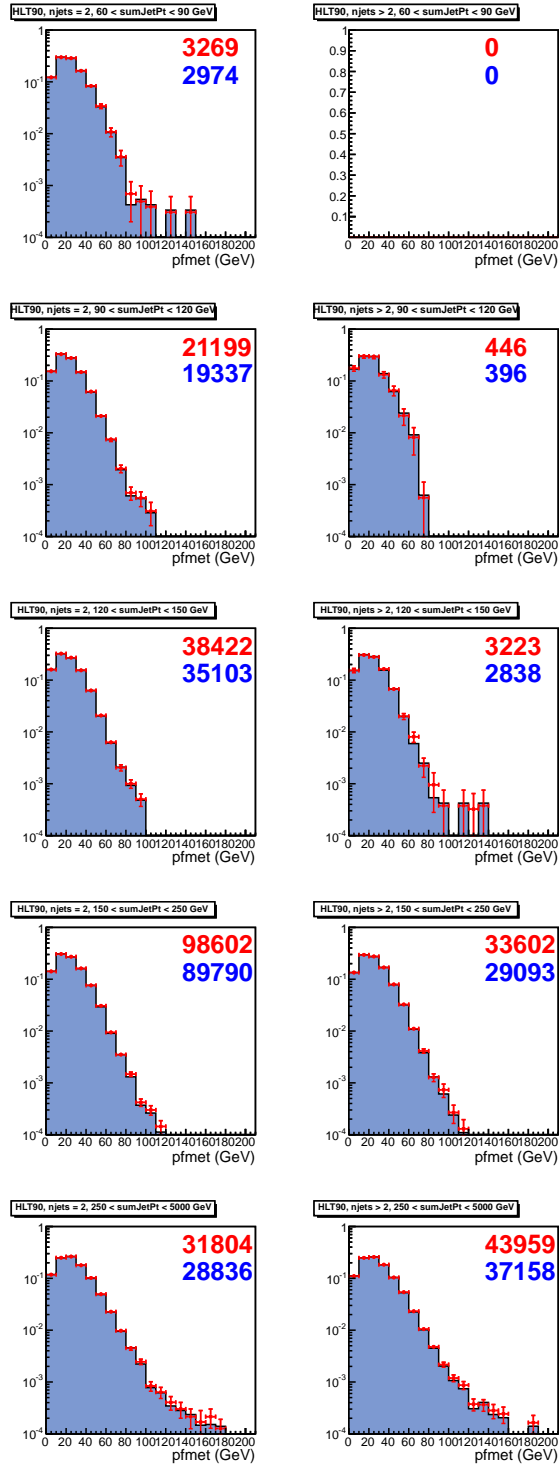


Figure 26: E_T^{miss} templates collected with the $p_T > 90$ GeV single photon trigger. The number in red (blue) indicates the number of entries in the template for the inclusive (targeted) analysis.